

The Development and Characterization of a Measurement Platform for the Evaluation of Aerosol Capture Devices

Yonatan Morocz

Dept. of Biomedical Engineering, McGill University, Montreal, Canada

Submitted: August 2023



McGill

A thesis submitted to McGill University in partial fulfillment
of the requirements of the degree of Master of Engineering

©Yonatan Morocz, 2023

Table of Contents

Abstract	4
Résumé	6
Acknowledgements	8
List of Figures and Tables	9
List of Abbreviations	11
1 Introduction	13
1.1 Motivation	13
1.2 Project goals	13
1.3 Contribution of authors	13
2 Comprehensive review of relevant literature	14
2.1 Aerosol particles	14
2.1.1 Physical properties and phenomena of aerosols	14
2.1.2 Aerosol sub-types	15
2.1.3 Aerosols and their role in disease	17
2.2 Aerosol capture devices	21
2.2.1 Filtration	23
2.2.2 Impaction	24
2.2.3 Centrifugation	25
2.2.4 Electrostatic sedimentation	26
2.2.5 Impingement	26
2.2.6 Microfluidic aerosol capture	27
2.3 Platforms for the evaluation of aerosol capture devices	27
2.3.1 Particle counting and measurement	28
2.3.2 Aerosol generation methods	28
2.3.3 Airflow sources	30
2.3.4 Fundamentals of a characterization platform	30
2.3.5 Complex characterization platform	31
2.4 Project rationale	32

3	Materials and Methods	33
3.1	Resin and prepolymer solution preparation	33
3.2	3D printer operation	33
3.2.1	FDM printing	33
3.2.2	LCD MSLA printing	33
3.2.3	DLP printing	34
3.3	Post processing of printed material	34
3.3.1	Surface treatments	34
3.4	Air tunnel	34
3.4.1	Hermetic seal evaluation	34
3.4.2	Particle measurement	35
3.4.3	Pressure measurement	35
3.4.4	Air speed and regulation	35
3.4.5	Aerosol particle generation	36
3.5	Macro photography	37
3.6	Microscope imaging	37
4	Results	38
4.1	CACD platform development	38
4.1.1	Design iterations, choices and rationale	38
4.1.2	Airflow sources	41
4.1.3	Material selection	42
4.1.4	Sensor selection and validation	44
4.1.5	Performance of the CACD platform version 5	46
5	Discussion	49
5.1	Requirement of a custom platform	49
5.2	Advantages and challenges of current approach	49
5.3	Comparison of particle detection methods	51
5.4	Comparison to existing evaluation platforms	52
5.5	Design iteration and evolution	52
5.6	Future directions	53
6	Conclusion	55
	References	55

Abstract

The transmission of SARS-CoV-2 via aerosol particles has been established during the pandemic, but remains an important topic of controversy. The analysis of the biological content of bioaerosols depends on aerosol capture devices, but existing devices are typically large and cumbersome, and were not widely available or widely used for analysis of SARS-CoV-2 aerosols. Better capture devices could help identify the prevalence of SARS-CoV-2 aerosols, and might also serve as the basis for non-invasive diagnostic of COVID-19 infection, and infectiousness. Significant efforts were devoted to develop compact and convenient aerosol capture devices (ACDs), including recently in our lab, however the capture efficiency and other performance metrics of these devices need to be benchmarked, which requires specialized equipment not readily available. Here we introduce a platform for the characterization of (small) aerosol capture devices (CACD) to benchmark them.

The CACD platform is 3D printed and can accommodate ACDs operating according different principles, is modular, can operate at pressures of up to 10 PSI (~ 70 kPa), measure particles from $0.2\mu m$ to $20\mu m$ in size, and accommodate airflow rates up to 100 L/min. It includes pressure sensors, anemometers and glass window for particle counting and sizing with minimal perturbation by phase doppler anemometry (PDA) both upstream and downstream of the ACD. Air containing aerosols enters the platform through one of 2 possible inlets, is directed through the quantification zone containing the pressure and particle sensors, and through the ACD, and exits through the outlet.

The thesis describes various challenges that were overcome in the design of the CACD such as generation of stable and precisely controllable airflow, the quantification of particle sizes independent of airspeed and pressure, the tunable generation of aerosol particles, and leakage which could all contribute to erroneous measurement results. Among the different airflow sources investigated, a regulator capable of self-feedback control was selected for its superior reproducibility. The measurements acquired from commercial air quality sensors varied with the pressure of the airstream, which was resolved by the adoption of PDA as the primary particle measurement system. Overall, great care was taken to develop and test mechanical interfaces between various components while preserving a hermetic seal throughout the CACD platform.

We evaluate the functionality of the CACD platform by measuring the aerosol capture efficiency and pressure drop of a previously uncharacterized impact-based ACD. The behavior of the recently developed impactor followed trends predicted by the stokes equation, with a capture rate of ~ 50 - 60% for 0.2 - $4\mu m$ particles and increasing up to 90% for particles above $6\mu m$. The PDA showed a coefficient of variation (CV) = 0.083 for particle measurements in the 0.2 - $5\mu m$ range

without an ACD present and a CV range of 0.07-0.4 with an ACD present. The reliability of the PDA was drastically improved following the setup of the automated motion stage to ensure sampling site accuracy. The CV for the pressure measurements was 0.28 at low sampling rates and 0.11 with an improved acquisition protocol. Further validation through testing ACDs with known performance is required for confidence in the quantitative results of the CACD platform. The presented CACD platform's sensitivity, range of operation, modularity, and potential for expansion make it a significant contribution to the field of aerosol research and capture device development.

Résumé

La transmission du SRAS-CoV-2 par les particules d'aérosols a été établie pendant la pandémie, mais demeure un important sujet de controverse. L'analyse du contenu biologique des bioaérosols dépend des dispositifs de capture des aérosols, mais les dispositifs existants sont généralement grands et encombrants, et n'étaient pas largement disponibles ou largement utilisés pour l'analyse des aérosols de SRAS-CoV-2. De meilleurs dispositifs de capture pourraient aider à identifier la prévalence des aérosols de SRAS-CoV-2 et pourraient également servir de base à un diagnostic non invasif de l'infection par COVID-19 et de l'infectiosité. Des efforts considérables ont été consacrés au développement de dispositifs de capture d'aérosols (ACD) compacts et pratiques, y compris récemment dans notre laboratoire, mais l'efficacité de la capture et d'autres critères de performance de ces dispositifs doivent être évalués, ce qui nécessite un équipement spécialisé qui n'est pas facilement disponible. Nous présentons ici une plateforme pour la caractérisation de (petits) dispositifs de capture d'aérosols (CACD) afin de les comparer.

La plateforme CACD est produite par impression 3D pouvant accueillir des ACD fonctionnant selon différents principes. La plateforme est modulaire, peut fonctionner à des pressions allant jusqu'à 10 PSI (~ 70 kPa), mesurer des particules de $0,2\mu m$ à $20\mu m$ et s'adapter à des débits d'air allant jusqu'à 100 L/min. Elle comprend des capteurs de pression, des anémomètres et une fenêtre en verre pour le dénombrement et la mesure de taille des particules avec une perturbation minimale par anémométrie à effet doppler de phase (PDA) en amont et en aval de l'ACD. L'air contenant des aérosols entre dans la plate-forme par l'une des deux entrées possibles, puis est dirigé vers la zone de quantification contenant les capteurs de pression et de particules, comme à travers l'ACD, et sort par la sortie.

La thèse décrit les différents défis qui ont été relevés lors de la conception du CACD, tels que la génération d'un flux d'air stable et contrôlable avec précision, la quantification de la taille des particules indépendamment de la vitesse de l'air et de la pression, la production modulaire de particules d'aérosol et les fuites qui pouvant contribuer à des résultats de mesure erronés. Parmi les différentes sources de débit d'air étudiées, un régulateur capable d'effectuer un contrôle par rétroaction automatique a été sélectionné en raison de sa reproductibilité supérieure. Les mesures obtenues à partir de capteurs commerciaux de qualité de l'air variaient en fonction de la pression du flux d'air, ce qui a été résolu par l'adoption du PDA comme principal système de mesure des particules. Dans l'ensemble, un grand soin a été apporté à la conception et au test des interfaces mécaniques entre les différentes composantes, tout en préservant un joint hermétique dans l'ensemble de la plateforme CACD.

Enfin, nous démontrons la plate-forme CACD sur un impacteur de base, en mesurant le taux

de capture des particules et la chute de pression à travers l'impacteur. Le PDA a montré un coefficient de variation (CV) de 0,083 pour les mesures de particules dans la gamme $0,2-5\mu m$ sans ACD présent et une gamme de CV de 0,07-0,4 avec un ACD présent. La fiabilité du PDA a été drastiquement améliorée suite à la mise en place d'un système de mouvement automatisée pour assurer la précision du site d'échantillonnage. Le CV des mesures de pression était de 0,28 à des taux d'échantillonnage faibles et de 0,11 avec un protocole d'acquisition amélioré. La sensibilité, la gamme de fonctionnement, la modularité et le potentiel d'expansion de la plateforme CACD présentée en font une contribution significative au domaine de la recherche sur les aérosols et au développement de dispositifs de capture.

Acknowledgements

First and foremost, I would like to thank my supervisor, Prof. David Juncker, for the motivation, support, and mentorship he's provided from the very start of my degree. I actually changed projects about four months into my degree and with his support the transition and initiation of a new project was seamless.

Many thanks to Dr. Andy Ng for his continued input on my project and insightful suggestions, Dr. Felix Lussier for his french help and comradeship on the second floor, help with experimental planning and microscopy. I would also like to mention Vahid Kharamzadeh for his help with 3D printing. I am also grateful to all the Juncker Lab members, in particular Geunyong Kim, Alan Huang, Molly Shen, Zijie Jin, Nick Chahley, Houda Shafique, Hugues Martin and Justin de Vries for always offering their help and feedback, their cakes, bread and camaraderie.

I would also like to thank Brandon Wallace in the Chemistry department at McGill University for helping with the early aerosol experiments. Additionally, Xavier Lefebvre from Polytechnique Montreal who was instrumental in the validation of the version 5 CACD platform

Lastly, I would like to express my appreciation to my friends and family. Brooke Turkalj for listening and supporting my rants about 3D printing. And thank you to my parents, and my siblings, for their constant encouragement and for always believing in me

List of figures

Figure 1: MODIS aerosol optical depth averaged over 10-year period 2001–2010.	pg. 16
Figure 2: SEM images of example aerosol particles.	pg. 17
Figure 3: Generation of aerosols in the human respiratory system.	pg. 18
Figure 4: Fraction of virus-laden droplets present in respiratory ejected droplets.	pg. 20
Figure 5: Photographs of the illuminated aerosol plume after flush initiation.	pg. 20
Figure 6: Schematic overview of a portable device to sample exhaled particles.	pg. 25
Figure 7: Representative illustrations of different aerosol capture methods.	pg. 27
Figure 8: Two different ACD evaluation platforms.	pg. 32
Figure 9: Design and fabrication of custom anemometer housing.	pg. 36
Figure 10: CACD platform versions 1-4.	pg. 38
Figure 11: CACD platform version 5 design with labelled components.	pg. 39
Figure 12: PDMS ACD sleeve molding components.	pg. 40
Figure 13: CACD platform with ACD during PDA measurement.	pg. 41
Figure 14: Measurements from CACD platform sensors.	pg. 42
Figure 15: Multi-material FDM constructs and threading fit tests.	pg. 43
Figure 16: Plots comparing Monocure resin and PEGDA resin.	pg. 44
Figure 17: Comparison of CO2 Click Model E with the HT-9600.	pg. 45
Figure 18: Particle count measurements using the HT-9600 for a simple impaction-based ACD.	pg. 45
Figure 19: Particle size distributions and capture rate for a flow restrictor and a classical impactor.	pg. 47
Figure 20: Pressure measurements before and after the capture zone for multiple levels of flow restriction.	pg. 48

List of Tables

Table 1: Aerosol particle sizes and associated volumes.	pg. 19
Table 2: Aerosol detection methods and associated properties.	pg. 22
Table 3: CACD platform (Version 5) specifications.	pg. 46

List of abbreviations

- **ACD** = Aerosol capture device
- **CACD** = Characterization of aerosol capture device
- **CV** = Coefficient of variation
- **FDM** = Fused deposition modelling
- **LCD** = Liquid Crystal Display
- **DLP** = Digital light processing
- **SLA** = Stereolithography
- **OC** = Organic carbon
- **BC** = Solid black carbon
- **AOD** = Aerosol optical depth
- **FFBB** = Fluid film, filament or bubble breakage
- **RTLF** = Respiratory tract lining fluid
- **TOF-MS** = Time of flight - mass spectrometer
- **LC-MS** = Liquid chromatography - mass spectrometer
- **ELISA** = Enzyme-linked immunosorbent assay
- **VOC** = Volatile organic compound
- **EBC** = Exhaled breath condensate
- **PCR** = Polymerase chain reaction
- **CCD** = Charge coupled device
- **PDA** = Phase doppler anemometer
- **SMPS** = Scanning mobility particle sizer
- **OPC** = Optical particle counter

- **IPA** = Isopropanol
- **PDMS** = Polydimethylsiloxane
- **PEGDA** = Polyethylene glycol diacrylate
- **PLA** = Polylactic acid
- **TPU** = Thermoplastic Polyurethane
- **ABS** = Acrylonitrile butadiene styrene
- **PETG** = Polyethylene terephthalate glycol
- **NPT** = National pipe thread

1 Introduction

1.1 Motivation

Aerosols are rapidly emerging as an attractive sample source for both pathogen detection and general biomarker exploration. To utilize this sample, aerosol particles must be efficiently sequestered and made available for post processing without damaging or altering the contents of the particles. However, the standard for comparing and evaluating these capture devices differ dramatically depending on the capture mechanism used, and the desired quantification metrics. Understanding the effects that design and capture parameters have on particle behavior is critical to the efficient development and benchmarking of such a device. This analysis requires a precise yet flexible platform for comprehensive device characterization.

1.2 Project goals

Initially the goal of this project was to develop a platform capable of comprehensively characterizing the aerosol capture device (ACD) developed in parallel within our lab. However it rapidly evolved to a modular test platform with the flexibility to adapt to many types of capture devices and analysis metrics.

1.3 Contribution of authors

Yonatan Morocz designed and performed all the experiments and analysis shown within this work. All structural designs and graphics not otherwise indicated were drawn and designed by Y. Morocz. Drs. Felix Lussier, Andy Ng and David Juncker provided guidance and feedback on designs and experiments. This thesis was written by Y. Morocz with feedback and suggestions by David Juncker.

2 Comprehensive review of relevant literature

2.1 Aerosol particles

2.1.1 Physical properties and phenomena of aerosols

The term aerosol particle is a general description which refers to any airborne particulate matter in a solid or liquid state. There have been disputes over the terminology and the specific size which qualifies a particle an aerosol. For this thesis the term aerosol will refer to particles with an aerodynamic diameter smaller than $100 \mu m$ in size unless specified otherwise. The aerodynamic diameter is an important descriptor of aerosol particles used in more advanced calculations of aerosol population dynamics and behavior. The aerodynamic diameter is calculated as the diameter of a spherical particle with the density of $1,000 kg/m^3$ (water) which has the same settling velocity as the particle in question.[18] A similar metric is the stokes diameter, which is the diameter of a spherical particle with the same density and settling speed as the particle in question.

Stokes law is the governing principle for the drag forces exerted by air or any fluid upon a particle with a specific velocity.

$$Stokes\ Law = F_d = 6 \pi \eta r v \quad (1)$$

$$terminal\ settling\ velocity = V_{TS} = \frac{\rho_p d_e^2 g}{18 \eta \chi} = \frac{\rho_0 d_s^2 g}{18 \eta} = \frac{\rho_b d_a^2 g}{18 \eta} \quad (2)$$

As the radius doubles, the surface area will go up 4x while the volume will go up 8x. The smaller the particle, the higher the surface area to volume ratio and consequently the evaporation rate.

$$Surface\ Area\ (Sphere) = 4 * \pi * r^2 \quad (3)$$

$$Volume\ (Sphere) = \frac{4}{3} * \pi * r^3 \quad (4)$$

The Knudsen number is a dimensionless number defining three dynamical regimes which govern the behaviour of aerosol particles. The mean free path is the average distance a particle can move within a medium before substantially changing its direction or energy.[18]

$$K_n = \frac{2\lambda}{d} \quad (5)$$

- $K_n \gg 1$: Free molecular regime:

Here aerosols are small compared to the mean free path, aerosol particles interact with their environment through ballistic collisions with gas molecules. They behave similar to gas molecules, following streamlines and undergoing diffusion due to Brownian motion.

- $K_n \ll 1$: continuum regime:

Here aerosols are large compared to the mean free path, so that the gas flows around the particles, the motion of the particles in this regime has significant momentum compared to their surroundings and doesn't precisely follow streamlines

- $K_n \sim 1$: transition regime:

Here aerosols behavior is complicated and varies between the continuum regime and the free molecular regime.

For mono-disperse spherical particles under $0.1 \mu m$ diameter every collision causes adherence. This type of thermal coagulation of sub-micron particles is called Smoluchowski coagulation. Larger aerosol collisions can result in complete or partial agglomeration or the fragmentation and generation of smaller aerosols depending on the fluid properties and impact conditions.

The Bernoulli principle will be mentioned here due to its relevance towards the development and design of the test platform and the capture device. Additionally, all fluids are assumed incompressible as air speeds are kept below Mach 0.6 and as such Bernoulli's equation for incompressible flow is shown below.

$$\frac{v^2}{2} + gz + \frac{p}{\rho} = constant \quad (6)$$

2.1.2 Aerosol sub-types

Primary aerosols are generated from liquid or solids directly through aerosolization, whereas secondary aerosols form through reactions between floating particles or gases, nucleating new aerosol particles or condensing on existing ones.

Aerosols can be formed through geological, atmospheric, biological and man-made activity. Common biological aerosols can carry viruses, bacteria, fungal spores, or pollen with typical respective diameters of $0.5 \mu m$, $1 \mu m$, $3-5 \mu m$, and $\sim 30 \mu m$. [26] They can be generated by expulsion from respiratory systems, plant and fungi ejection, the movement of liquid bodies or sheared from liquid surfaces by rapid air movement.

Humanity produces aerosols in abundance, with combustion processes at the top of the list, producing sub-micron carbonaceous aerosols such as organic carbon (OC) and solid black car-

bon (BC).[35] Aerosols containing nitrates and sulfates can also be formed from other sources of urban/industrial emissions, especially in heavily populated territories.

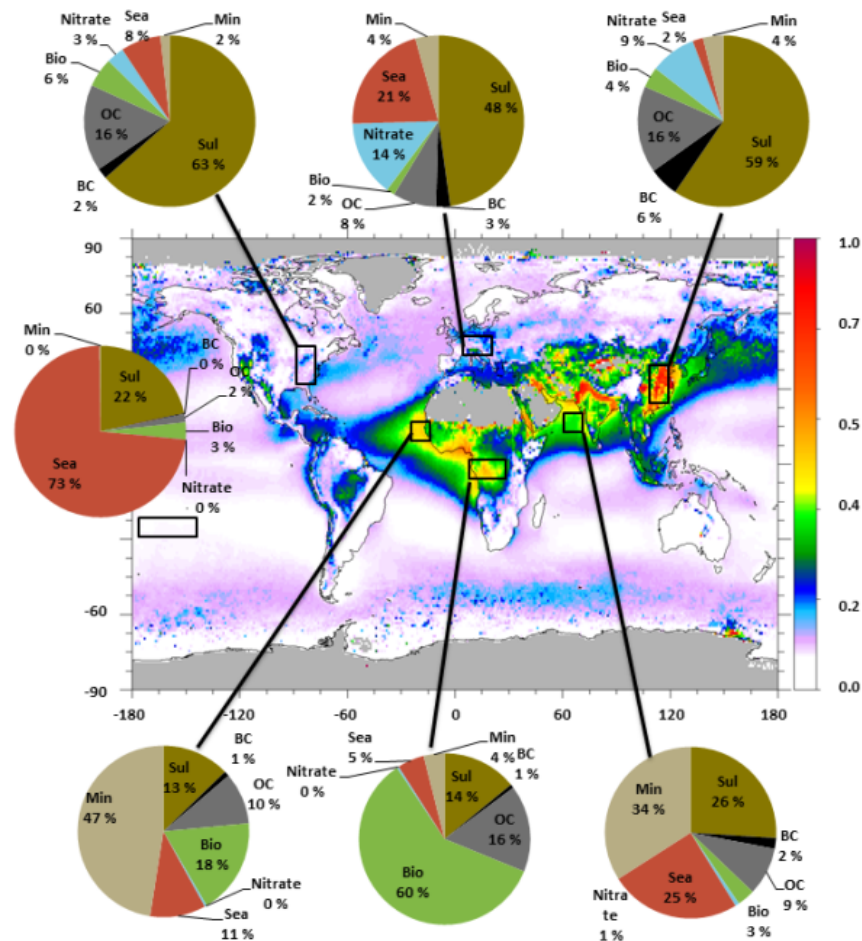


Figure 1: MODIS aerosol optical depth [AOD (550 nm); dimensionless] averaged over the 10-year period 2001–2010.[38] Pie charts show how various aerosol types contribute to the total AOD for different regions, as estimated by a global aerosol model.[34][35] *Reproduced with permission from Nature Education*

Mineral based aerosols comprise the majority of atmospheric aerosols which due to their large surface area and reactivities are known to impact macro-climates.[7] All atmospheric aerosols scatter incoming solar radiation, and many including BC also absorb radiation. Scattering aerosols have an overall cooling effect by reducing the intensity of radiation reaching the planet, while absorbing aerosols have a warming effect, especially if they are high in the atmosphere above reflecting clouds.

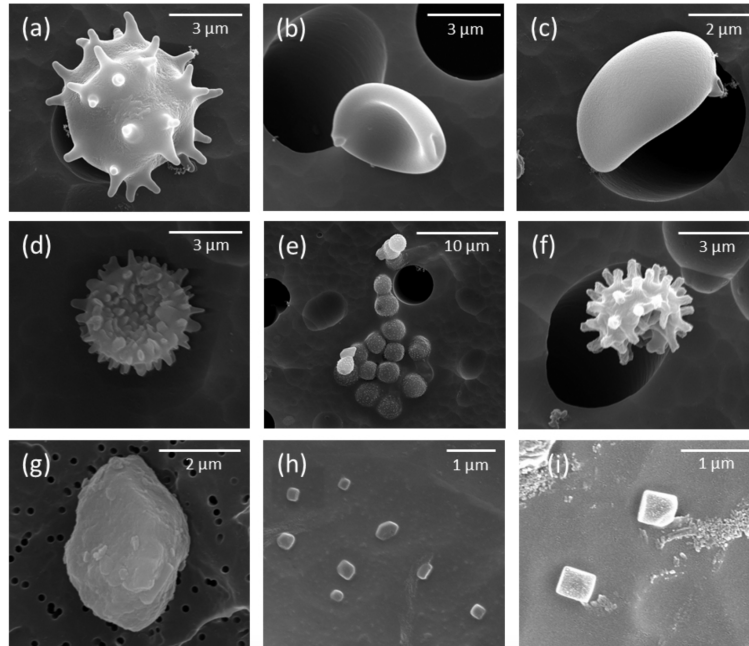


Figure 2: SEM images of example aerosol particles: (a-c) basidiospores, (e) spores coated with sea salt, (d-f) ascomycota spores, (g) mineral dust, (h-i) sea salt formed particles from ocean winds.[49] *Reproduced with Creative Commons Attribution 3.0 License*

2.1.3 Aerosols and their role in disease

Aerosol particles are a central vector for many pathogens to travel between hosts, this can be in the form of ejecta during expiration or even aerosolization of fecal particles in commercial toilets.[12] Aerosol transmission is in part responsible for the societal burden of lower respiratory infections, which are the 4th leading cause of death worldwide.[53] Aerosol transmission contributed to the spread of the recent 2019 SARS-CoV-2 pandemic, the 2012 MERS outbreak, the 2009 H1N1 pandemic, and the 2003 SARS outbreak.[45, 50, 46, 31] Healthcare facilities are especially prone to outbreaks of airborne pathogens as they contain a high density of susceptible individuals often undergoing procedures which can lead to product of aerosols.[4]

Aerosols can be generated in the human respiratory tract through two main methods, turbulent aerosolization and fluid film, filament or bubble breakage (FFBB) shown in Figure.3 .[33] Turbulent aerosolization has been defined as shear-induced surface wave instability, where particles are stripped from fluid films along respiratory surfaces. When air sweeps past a liquid film it can cause fine ripples to form and evolve into strands which fragment into a poly-disperse population of particles following a gamma distribution.[24] This typically occurs during high velocity respiration such as coughing. FFBB occurs in the deep bronchioles, during the vibration of the vocal cords in the larynx as well as the contact and separation of the lips and tongue with teeth during speech.

Contrary to what turbulent aerosolization alone would suggest, there is an asymmetry in particle generation with respect to the breathing cycle. The majority of aerosol particles in the lungs are generated during the inhalation and not during the exhalation. This is due to FFBB, wherein the bronchioles composing the deep lung collapse upon full exhalation and then during inhalation they expand, forming thin films or bubbles between the previously touching surfaces. These thin films then burst and fragment into particles which are exhaled upon the completion of the breathing cycle.

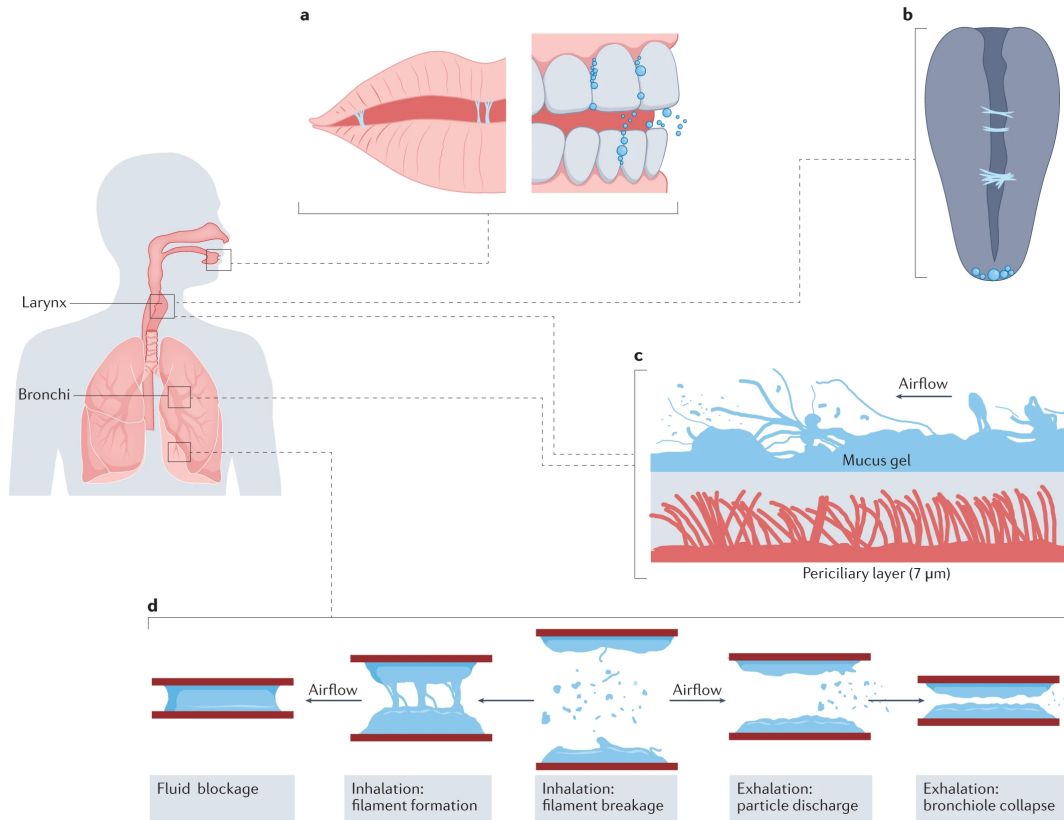


Figure 3: Generation of aerosols in the human respiratory system. a) Fluid film, filament or bubble breakage (FFBB) in the mouth during speech.[14] b) FFBB due to filament formation at the vocal cords. c) Turbulent aerosolization of viscoelastic mucus from the airway lining in the larynx and large bronchi due to turbulent airflow, based on snapshot of ligament-mediated fragmentation of viscoelastic liquid presented in ref.[24] d) FFBB in small airway bronchioles due to clearance of fluid blockages formed during exhalation and airway reopening.[33] *Reproduced with permission from Springer Nature*

The particles generated through turbulent aerosolization or FFBB are both derived from the respiratory tract lining fluid (RTLFL). This contains aqueous components as well as mucins, non-mucin proteins, salts, cellular debris and any other cells or pathogens which reside in that fluid. Additionally, saliva, nasal secretions, blood from oral lesions or food debris can also be present

in the aerosolized particles.[22] The biological mass to total mass proportion of these aerosols is 1-10%, which combined with their high surface area to volume ratio, leads to rapid desiccation as water and other volatile components evaporate. The remaining aerosol nuclei typically has a diameter of 30-50% of the original microdroplet which corresponds to $\sim 1/27$ th to $1/8$ th of the original volume (Table.1)[1].

Table 1: Aerosol particle sizes and associated volumes.

Diameter of Particle	100 nm	1 μm	10 μm	100 μm	1 mm
Volume of Particle	0.524 aL	0.524 fL	0.523 pL	0.523 nL	0.523 μL
Surface to Volume Ratio (μm^{-1})	60	6	0.6	0.06	0.006

Different patients have vastly differing RTLF viral loads, determining which particle sizes pose a transmission risk as shown in Figure.4. At a viral load of 10^6 only $\sim 0.07\%$ of $10\mu m$ particles will contain a virus, but at an individual viral load of 10^8 , $\sim 7\%$ of $10\mu m$ will contain at least one virus.[1] Smaller particles are theoretically better vectors as they have longer settling times and penetrate deeper into the lung alveoli. However, the virus distribution is assumed proportional to droplet volume, which decreases cubically as particle diameter decreases, favoring larger particles.[1] Although there is disagreement on which particles are the most relevant to disease transmission, the strongest case is made for particles in the mid-range $\sim 2 - 8\mu m$ as larger particles experience shorter air residence times and smaller particles may not contain any pathogenic particles.[42][2][11] $\sim 5\mu m$ particles are present in high numbers, have sufficiently large internal volumes and lengthy airborne lifetimes to be considered the dominant factor in aerosol disease transmission.

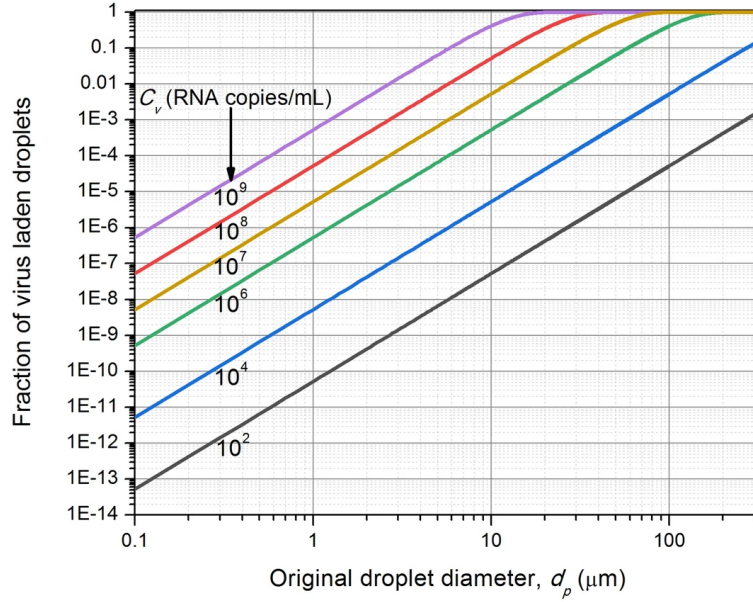


Figure 4: Fraction of virus-laden droplets present in respiratory ejected droplets, as a function of droplet size and viral load in the fluid.[1] *Reproduced from Sprinter Nature with Creative Commons Attribution 4.0 License*

Recent work has also highlighted other methods of aerosol generation relevant to disease transmission, including plumes of pathogen containing aerosols produced by flushing toilets (Figure.5).[12] Pathogens present on the walls of a toilet or within the rinsing water can persist after many flushes and can create respiratory risks within confined lavatory environments. Other sources of pathogenic aerosol generation will be discovered and highlighted as this field continues to grow.

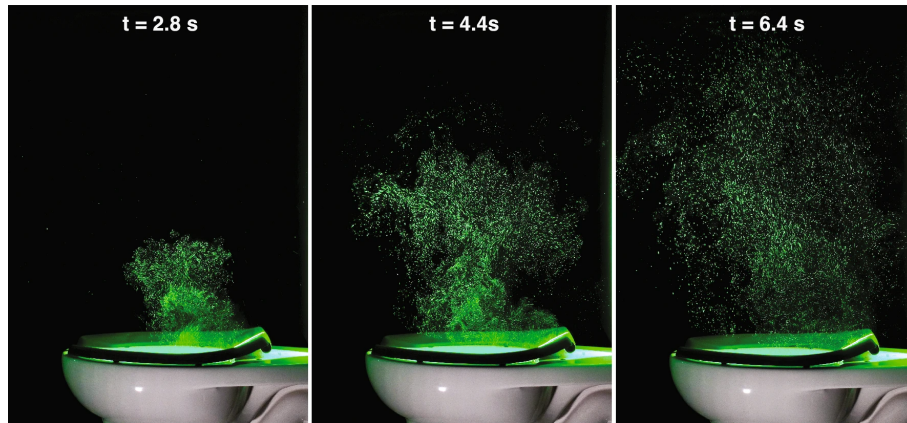


Figure 5: Photographs of the illuminated aerosol plume at $t = 2.8$, 4.4 , and 6.4 s after flush initiation. For these images a continuous wave laser and a commercial color camera was utilized; the images show the illuminated plume as it appears to the human eye in the laboratory.[12] *Reproduced from Sprinter Nature with Creative Commons Attribution 4.0 License*

Prior to the SARS-CoV2 pandemic, interest in aerosol analysis as an informative tool had already been rising. A 2017 technical standard by Horvath et al. highlighted several existing studies which had utilized aerosols for the detection of proteins and phospholipids.[19] They found the composition of aerosol particles to be $\sim 25\%$ proteins and $\sim 75\%$ phospholipids, in sufficient quantities for both exploratory TOF-MS and targeted ELISA based assays. Smokers and non-smokers were the subjects of another such investigation, which reports a dose-response relationship between tobacco consumption and variations in mass spectra obtained from exhaled particles.[6] Qualitative analysis showed that a higher molecular response of phosphatidylcholine species in captured aerosol particles strongly associated with poor lung function. Another publication applied SDS-PAGE and LC-MS in an exploratory approach based on captured aerosol particles and identified 124 unique proteins.[5] For specific analytes in the RTLF, aerosol particle capture can be the most effective sampling method. Particle capture has shown a superior detection rate for surfactant protein A compared to EBC and serum analysis with an increased specificity.[28]

2.2 Aerosol capture devices

Non-destructive aerosol detection

There is a major difference between simply detecting, sizing or optically analyzing an aerosol particle compared to actually capturing or sequestering the particle so that its contents can undergo further processes. There are a very large number of methods which use either light or other non-interfering methods to obtain information about a single or population of aerosols.[30][21] This includes the phase doppler anemometry system which we used in our own work. A summary table detailing some of these methods from a review by Li Et Al. is included below (Table.2), but further elaboration is outside the scope of this thesis. [30]

Table 2: Aerosol detection methods and associated properties.

Measurement Type	Detection Principle	Measured Parameters	Particle size range (μm)
Light Induced Fluorescence (LIF) (1–3 channel)	Fluorescence and elastic scattering	Particle size, fluorescence intensity (1–3 channel spectral resolution)	~ 0.5 to 10–50
LIF (multichannel)	Fluorescence (and elastic scattering for some instruments)	Particle size, fluorescence intensity (8–32 channel spectral resolution)	~ 0.5 to 10–100
LIF (multichannel) + holography	Fluorescence + elastic scattering + holography	Particle size, fluorescence in multiple channels, holographic images	~ 0.5 to 100
LIF (multi-channel) + LIBS + elastic scattering	Fluorescence + LIBS + polarized elastic scattering	Particle size, fluorescence intensity, elemental composition, and absorption	~ 0.5 to 10
Optical microscopy	Optical microscopy or high-definition photography	Microscope images	5
Elastic scattering	Elastic scattering	Forward and side scattering	10
Raman spectroscopy	Raman scattering (+ background fluorescence)	Images from which Raman spectra are extracted	10
Mass spectroscopy	Mass spectrometry	Mass spectra of fragment ions from single or ensembles of particles	~ 0.05 to 5
Breakdown spectroscopy	Atomic spectroscopy	Atomic spectra	1 to 100

Aerosol particles vs EBC vs VOC

The main vectors considered for breath analysis are volatile organic compounds (VOC), exhaled breath condensate (EBC) and aerosol particles. Although these sample types can overlap in their generation sites within the body, they differ vastly in their applications, limitations and the physical principles upon which they depend.

Exhaled VOCs are gaseous molecules which can provide information regarding microbes present in the body as well as the overall physiological state of the subject and their cells.[3] Compounds such as acetate, propionate, short chain fatty acids (SCFAs), alcohols, propanols, hydrocarbons,

aldehydes, ketone terpenes and many more have been detected in exhaled breath samples. While very informative about specific biochemical processes and physiological states, the information gained from VOC capture is limited when compared to particle capture. VOCs cannot provide the genetic material of a pathogen, specific protein samples or feed into any process requiring a physical sample. However, due to their ease of collection, they can be considered a complementary sample type to particulate matter for understanding the complete physiological state of a patient.

EBC is a robust sampling route which collects multiple components of exhalate through cooling mediated condensation of air. As the high humidity, body temperature air is cooled, it causes moisture from the air to condense onto the surfaces within the device as well as nucleate onto existing aerosol particles. EBC sequesters aerosol particles, RTLF, water soluble VOCs as well as the distilled water vapor from the exhalate.[13] EBC is a powerful sample source which has been long considered for pulmonary disease monitoring and successfully implemented in conjunction with RT-PCR recently to detect SARS-CoV2 with a 86% detection rate.[27][40] However, a significant challenge with EBC is the dilution of the aerosol particle sample by a factor of 2,000 - 10,000 due to the condensation of exhaled water vapor.[27][20] EBC also requires the cooling of air and typically a larger device than some particle capture solutions. This makes it less suitable for rapid sample acquisition at the point of care.

Aerosol capture provides information that VOC capture cannot and retains an improved concentration of the sample when compared to EBC. The following sections will review existing aerosol capture principles, their benefits and shortcomings.

2.2.1 Filtration

Filtration relies on a porous material to prevent particles above a specific pore diameter from passing through with airflow (Figure.7).[30][51] Filter structures can consist of interwoven fibers, packed beads, monolithic porous membranes or other frameworks. Large industrial filters used in HEPA systems and small filters in cigarette butts all use the same principle to sequester particles from airflow. However, since the pore size of a filter is what determines the size of particles captured, this variable is preset from the fabrication stage of the device. Additionally, as particulate matter is captured and blocks pores, filters often undergo clogging, increasing their flow resistance. Similarly to impaction based devices, filters suffer from difficult extraction, and as such are more suited to *in situ* analysis. Modern air filters often take advantage of electrostatic effects to attract particles to the fibers which are smaller than the actual pore sizes of the filter.[8]

Recent publications have developed various fiber coatings for improving the characteristics of filters. Bifunctional polyester/aluminum fibers have shown exceedingly high capture rates

(99.9%) of *E. coli* particles at a flow velocity of 3.4 cm/s through a combined electrostatic filtration approach.[8] These same fibers also deactivate the captured pathogens via the growth of aluminum crystals.

2.2.2 Impaction

The principle behind impaction is that aerosol particles above a certain mass cannot adjust to changes in the flow of air and thus impact upon a solid substrate (Figure.7). [30][51] The specific geometry and the airspeed determine the size of particles a impaction based method is capable of capturing. The simplicity of capture principle and ease of use are the primary benefits, which translate to scalable devices with the potential for high air throughput. However, these devices often struggle from poor sample extraction and viability for post capture applications. Often for complete extraction, excessive washing solutions are required, decreasing the concentration of the analyte in solution. This is not an issue if imaging and quantification is done *in situ*, but limits the utility of this method for specific techniques. Additionally, if capturing onto a solid dry substrate for extended periods of time, bioaerosol desiccation can cause samples to deteriorate.

A recent study used impaction based capture upon a transparent substrate in combination with a fluorescence imaging setup to capture both standardized polystyrene latex (PSL) beads and *E. coli* containing particles.[9] They achieved a flow rate of 10 liters/min and a particle cut-off diameter (d_{50}) of $\sim 0.84\mu m$. However, this device is limited in its applications as the sample is not extracted from the impaction plate, it is imaged and cultured *in situ*.

A Sars-COV2 breathalyzer was published by *Stakenborg Et al.* which uses impaction based capture to sequester aerosol particles within a disposable sampling device (Figure.6).[44] They employ silicon wafer microfabrication and deep reactive ion etching to fabricate two layer and monolithic versions of their impaction device. A patient exhales through the device repeatedly to collect the aerosol particles, then the sieve is processed *in situ* using qPCR to quantify the viral load present. Their design uses capillary filling to deliver PCR mix to all the necessary areas of the chip. This design minimizes the liquid necessary to retain high concentration and avoids dealing with sample extraction from the impaction substrate. With dimensions of $13mm * 13mm * 30\mu m$, the minimum volume of their device is $\sim 5\mu l$ or more if the pores are filled as well. However, their design requires a relatively complex fabrication process involving silicon microfabrication, putting it out of reach of organizations without the means to equip specific facilities and acquire expensive materials.

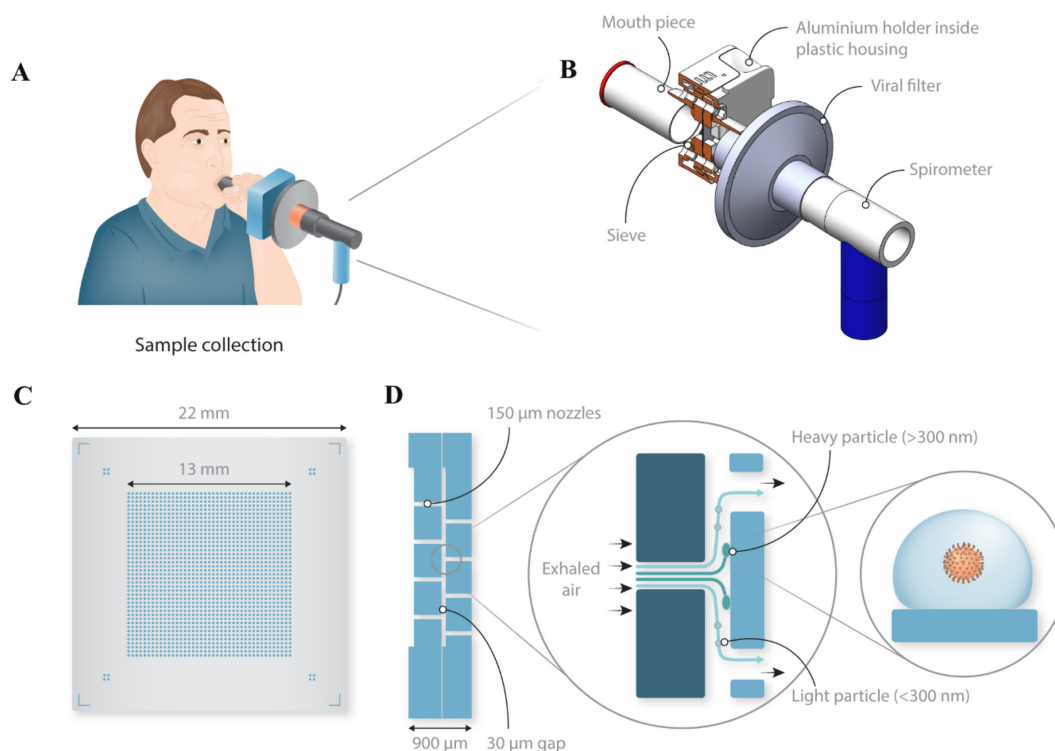


Figure 6: a) Schematic overview of the portable device to sample exhaled particles. b) Design of the disposable sampling device. (C) Schematic top-view of the final sieve, $22 \times 22 \text{ mm}^2$ in size, consisting of an array of 1600 nozzles with a diameter of $150 \mu\text{m}$. (D) The non-integrated, non-monolithic impactor consists of two sieves stacked on top of each other, creating a gap of $30 \mu\text{m}$ between the two arrays of holes. Exhaled particles are collected on the bottom sieve by inertial impaction, while air and very small particles ($\leq 300 \text{ nm}$) are directed to the outlet nozzles and exit without impacting.[44] *Reproduced from Elsevier with Creative Commons Attribution CC BY-NC-ND 4.0 License*

2.2.3 Centrifugation

Centrifugation based capture methods use particle inertia and differences in centripetal forces to guide particles into capture areas.[30][51] A cyclone is a typical centrifugation based capture method which can often be seen in commercial woodworking shops to separate sawdust from large volumetric air flows (Figure.7). This high throughput and continuous flow is the main advantage of centrifugal aerosol capture methods. However, typically when capturing micron scale particles, a thin liquid film is generated along the outside of the cone for improved particle sequestration. This requires external pumps and precise control of volumetric airflow and liquid manipulation to maintain the thin film of liquid. The large volume of liquid used to create this thin film can be recycled through the system, but even with that adaptation the concentration of analytes is still low. Cyclones are most suitable for long term collection of large volumes of air in

stationary environments, where they can overcome the concentration challenges and accommodate their peripherals.[23]

Cyclones are not the only form of centrifugal capture, as some microfluidic devices use the same principle but on a 2D plane rather than a 3D cyclone pattern. [10] These miniaturized centrifugal devices improve the otherwise poor capture rate of cyclones for particles in the $0.3\mu - 3\mu m$ range at the cost of reduced throughput. However, this particular example was only capable of reaching a maximum airflow rate of 1.2 L/minute.

2.2.4 Electrostatic sedimentation

Active electrostatic capture methods use an air ionizer supplying a high voltage to electrically charge aerosol particles. These charged particles then enter an electric field provided by positive and negatively charged components. Depending on the charge of the particles, they will be either attracted or repelled by these components, which causes them to impact upon the desired capture substrate.[30][51] These capture devices can be fabricated using generally available cheap components which makes very valuable and effective in resource limited environments.[36] Electrostatic capture methods don't require high resistance airflow paths and as such they have some of the lowest pressure drops among capture devices. This makes them suitable for breath sampling as it doesn't require high pressure exhalation from a patient. However, the ionization of aerosol particles has been shown to modify or destroy some pathogens, affecting their viability for further analysis post capture.[17] All active electrostatic methods require electricity, and while they typically consume less power than active pumping solutions, they are still more dependant than filters or passive methods.

2.2.5 Impingement

Impingement sequesters aerosol particles in a liquid medium typically by bubbling air through a liquid (Figure.7).[30][51] This increases the surface area of the liquid to air interface so as to improve the transfer rate of particles into the liquid. Impingement has the advantage of capturing aerosols in a liquid medium, which inherently improves the sample viability compared to other sampling. However, when capturing with high air flow rates, the higher liquid shear forces can negate this advantage and also result in reduced viability. Another inherent advantage of capturing in liquid is that the extraction of the sample is simplified compared to impaction or filtration based devices. This same advantage becomes the main limitation of impingement, the sample is heavily diluted due to the relatively large volume of liquid necessary. This can be remedied by long term sample collection or extremely high volumetric throughput of air. Both of those options render

impingement difficult to apply to patient diagnostics and more suitable for air quality monitoring. A 2017 publication illustrated a stereotypical impingement device with 5-20 ml of capture volume, and a flow rate of 12.5 liters/min.[55] However as a consequence of the limitations of impingement devices, they required at least 15 minutes of aerosol particle collection for sufficient capture.

2.2.6 Microfluidic aerosol capture

Microfluidic ACDs usually fall within the categories described previously, but they take advantage of the principles of microfluidics to improve their sensitivity, capture rate, and portability.[29] There are microfluidic adaptations of impaction based devices, bubblers, cyclones and electrostatic capture devices.[52] However, most microfluidic devices for the capture of aerosols depend on external pumps or detection components which complicate their operation by general consumers and limit their utility at the point of care. These microfluidic devices excel at providing high concentration samples for analysis as they typically require far less liquid than traditional capture devices. Integrated capture and detection devices have started to enter the field, but they lack certain aspects which an all-in-one solution would have. They either possess low throughput, require complex peripherals, or are paired with limiting detection and analysis methods.

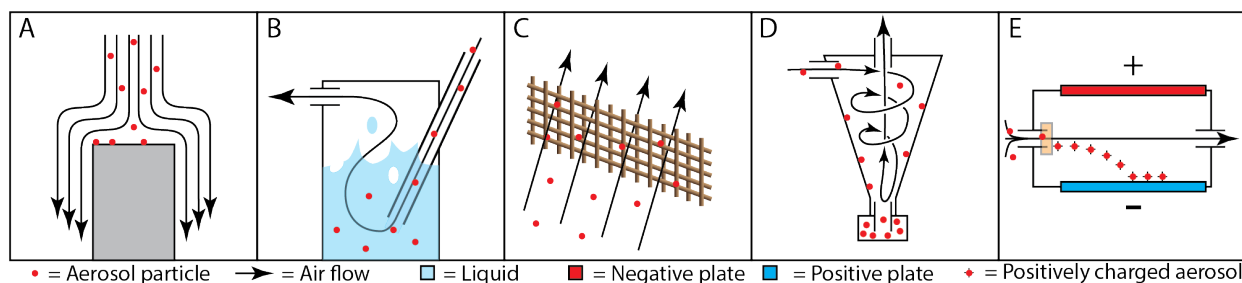


Figure 7: Representative illustrations of different aerosol capture methods.[30] a) Impaction of aerosols upon a solid substrate. b) Impingement of aerosols within a liquid medium. c) Filtration of aerosols within a fiber network. d) Centrifugation of aerosols in a cyclone. e) Electrostatic precipitation of aerosol particles after corona charging.

2.3 Platforms for the evaluation of aerosol capture devices

Comparing ACDs reliant on varied physical phenomena and behaviors is challenging due to the heterogeneity in their throughput, size and output format. Most if not all novel aerosol devices published implement custom solutions with tools that fit their specific needs but that may have trouble adapting to quantifying other capture devices. This hinders the fair comparison of devices as each platform is ideally suited for the characterization of a specific device. However, this can also be

the advantage of designing a custom evaluation platform as one can tune the instrumentation to highlight the features of the specific device in question.

2.3.1 Particle counting and measurement

There exist two main categories of particle counting devices that will be reviewed in this thesis, optical methods and physical methods. Optical methods typically fall into the following descriptions; light blocking methods, scattering methods and direct imaging setups. Light blocking methods rely on preventing light from reaching a CCD or photo multiplier tube and therefore signalling the presence of a particle, variations of this method can be implemented to also provide the sizing of particles. Scattering based methods such as the one used in this work (DualPDA) use the scattering of incident light from particles to highlight the size and speed of detected particles.[37, 43] High end scattering based methods can detect particles all the way down to 10-100 nm range based on Rayleigh theory, but typically have a submicron threshold for particle sizing. Direct imaging is the simplest of the optical methods and relies on the illumination of the particles by a light source and the direct imaging of the particle flow. This method typically has a particle diameter threshold of $1\mu m$, but can be the easiest to implement. All the optical methods described above provide the distribution of particle sizes within their range.

Two physical methods will be described herein, the filter blocking method and electrical pulse impaction. The filter blocking method measures the resistance across a filter, as aerosol particles are captured in the filter and the pores are occluded, the resistance will increase. The limitations of this method are that it cannot differentiate between sizes and the filter is clogged overtime, meaning that the instrument has to be recalibrated often. Electrical pulse impaction is a destructive method of aerosol counting which charges particles electrostatically and then impacts them upon a metallic substrate.[16] Electrical impulses are imparted to the substrate by particles above $2.5\mu m$ allowing the determination of the particle size distribution.

Condensation nucleation is a supplemental method that can be paired with the optical methods above to improve their size resolving capabilities.[39] It uses cooled supersaturated gas to promote the condensation of liquid onto the particles, increasing their size prior to detection. This method can be implemented to enlarge and image particles down to 2 nm in size.

2.3.2 Aerosol generation methods

As reviewed earlier, there are many different biological and non-biological methods for aerosol generation and just as many unique aerosol particles. Devices exist to generate both solid and liquid aerosol particles as well as poly disperse vs monodisperse aerosols. Additionally although

not part of the aerosol generation, it must be taken into account whether recirculation of airflow is necessary or fresh aerosols need to be injected constantly. Some of the particle generators below allow for monodisperse or polydisperse generation, but there are other supplemental devices such as a differential mobility analyzer which can be used to control for a specific size within a polydisperse distribution of aerosol.

Ultrasonic nebulizers are the most common in consumer households as they are present in many humidifiers as well as medication dispensers.[25] An ultrasonic nebulizer works through the formation of capillary waves on the surface of a fluid through the vibration of a solid substrate, initiating the breakup of smaller wave peaks into jets of small droplets ($100\text{nm} - 50\mu\text{m}$). Ultrasonic nebulizers are also present in industrial mass spectrometers and spray pyrolysis applications.

Collision nebulizers also known as pneumatic nebulizers or jet nebulizers are widely employed in aerosol and aerobiology research, occupational hygiene, and industrial filtration evaluation.[15] A high speed jet of compressed air flows through a small orifice to create a reduced pressure zone which siphons liquid into the flow and shears it into thin sheets and droplets. There are many variations of this standard method listed below:

- Blaustein Liquid Atomizing Module (BLAM): A specialized nozzle for jet nebulizers to control the size distribution of particles by altering the distance between particle jet and impaction within the generator. Can be poly or quasi mono disperse.
- Sparging Liquid Nebulizing Generator (SLAG): Polydisperse, reduced shear forces for microorganism aerosolization. Gently bursts thin films to generate aerosols rather than shearing or impaction.

Solid aerosol generation is not the topic of this thesis, however several existing methods are highlighted below:

- Wright Dust Feeder (WDF): Selectable output size with large concentration range. Consists of a scraper moving along a packed substrate bed to control the aerosolization rate and size.
- Vilnius aerosol generator: Fluidized bed with particle size range of ($0.01\mu\text{m} - 50\mu\text{m}$). Vibrating bed prevents particle agglomeration and maintains size consistency.
- Rotating brush generator: Typically used for the generation of test aerosols from powders, pollens and spores. A brush rotates against a packed powder substrate while a high flow of air passes through the brush carrying the newly separated particles to the outlet.

There are also a number of model systems which can be considered specifically for biological aerosols. The simplest of these method consists of RNA or protein laden aerosol particles, which following capture can be analyzed using PCR or ELISA. More complex and biologically relevant models of bioaerosols include culturable bacteria, or phages capable of affecting bacterial populations after capture.[48] These models allow for the assessment of pathogen viability following the aerosolization and capture process and not only the content of the particles.

2.3.3 Airflow sources

Characterization platforms for aerosols typically require an airflow source, although some methods do exist which conduct passive sequestration from ambient air. This airflow can be provided either by compressed air from a tank or a blower fan, or through the use of a vacuum to pull air through the device. The main advantage of using a vacuum is the avoidance of turbulence which may be caused by fan blades or the input propulsion of the air. However, the majority of characterization devices still use compressed air due to its standardization in purity, reduced fluctuations and ease of control.

There are many variations of industrial air and mass flow regulators which will not be reviewed in this thesis, however the principle of set pressure vs set volume/mass will be reviewed. Typically these regulators can either produce a set pressure at their outlet, or force a set volume of air through up until the outlet reaches the pressure of the inlet. For characterizing ACDs, setting the volumetric flow rather than the pressure is valuable as many devices have high flow resistances. To best characterize the device it is important to know the precise volumetric flow rate through the device and a set pressure would not provide this information. When paired with pressure sensors these regulators give a clear image of the airflow occurring within the platform.

2.3.4 Fundamentals of a characterization platform

A novel filtration based capture device was published in 2018 and the platform shown in Figure. 8B was assembled to fully characterize the device.[8] This setup has an additional electric field forming features prior to the capture device in the airflow to enhance the electrostatic capture abilities of their filter. They implemented standard pre-filtration and drying of the air entering the aerosolizer as well as drying after aerosolization before entering the capture area. This is explained by their use of a jet nebulizer with bacterial matter as their aerosolized particle. To effectively size the particles they are capturing and take advantage of the electrostatic effects, excess liquid from the aerosolizer is evaporated. Their quantification platform consists of valves before and after the capture area which can redirect flow to a aerodynamic particle sizer (TSI

Model 3321). This device uses scattering and TOF measurements to obtain the size distribution of particles. The main issue with this approach is the separation of the quantification site from the capture device, the concentration and size of the particles can change from the capture site to the detection site. While this configuration is representative of the core elements required for such a characterization platform, the ideal scenario is to perform quantification as near to the capture device as feasible, ensuring a more accurate representation of real measurements. A similar but simpler configuration was developed for a 2023 publication on the effect respiratory mask sterilization had on filter performance.[47] This work utilized a scanning mobility particle sizer (SMPS, Model-3080, TSI) for particle measurement, a differential pressure sensor (FLUKE 992) and a Kr-85 Aerosol Neutralizer (TSI-3054A) for removing particle charge. Similarly to the first paper mentioned they also implemented particle and relative air humidity control.

2.3.5 Complex characterization platform

In a 2021 publication, the development of the air and liquid handling platform shown in Figure.8 was carried out to characterize a complex of virtual slit impactor.[54] This was chosen to illustrate how more complex characterization platforms are sometimes required, but still incorporate the same basic elements. The principle of the virtual impactor relies on accurately controlling recirculating airflow layers and manipulating pressure to control the flow paths of particles within the isolation zone. Solid aerosol particles were chosen for this platform, generated by a SAG410 (TOPAS) and a EP-NGs20 metal nanoparticle generator for particles smaller than 150 nm. They use a differential mobility analyzer to purify for monodisperse particles prior to the virtual impactor. However, this seems to be counter productive as they cannot see the effects that the virtual impactor has on particle sizes outside of the target range.

Similar to the previous method they measure the aerosol particle size distribution upstream and downstream of the virtual impactor, however used a dual quantification system rather than a single device to ensure accuracy. A SMPS (Model-3938, TSI) and a optical particle counter (OPC)(Model 1.109, GRIMM) were used. However they implemented multiple valves and operations between the impactor and the measurement devices similar to the previous platform.

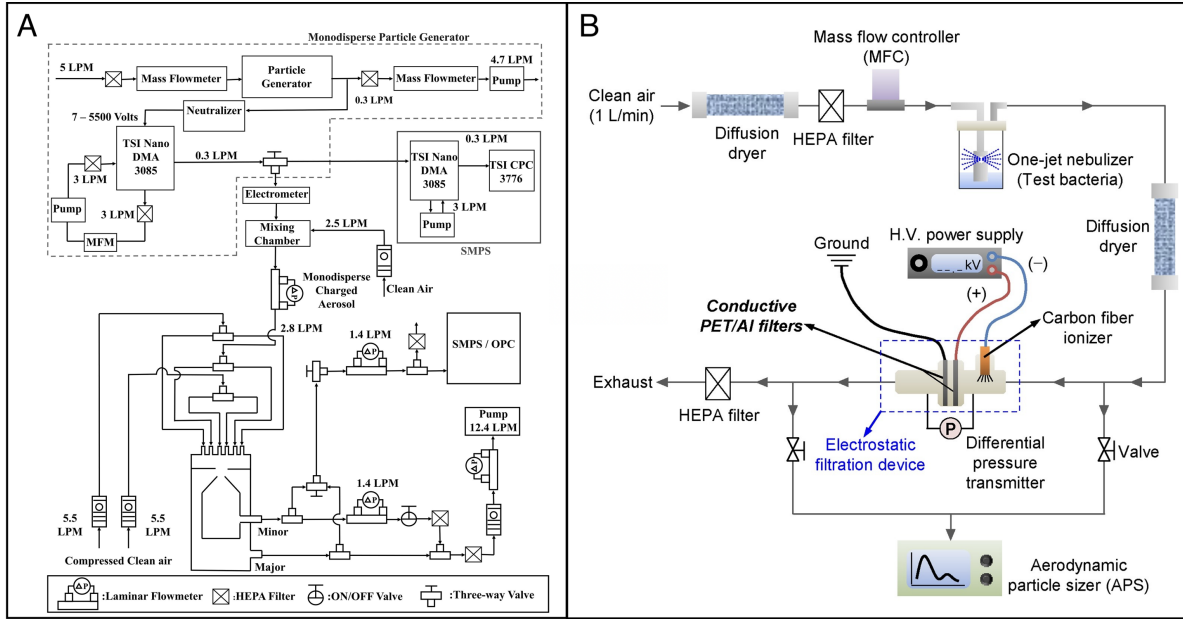


Figure 8: Evaluation platforms utilized in two distinct publications regarding aerosol capture. a) The complex system necessary for a virtual impaction based particle size separation device.[54] b) The test setup for the characterization of a anti-microbial air filter.[8] *Reproduced with permission from Elsevier*

2.4 Project rationale

Our lab required a characterization platform to evaluate the performance of a novel capture device and due to the heterogeneity of the solutions implemented in the literature a custom configuration was required. These differences hinder the reproducibility of results and lead to biased analyses of capture devices. A number of existing designs were analyzed for their core components and referenced throughout the design process. The proposed platform presented here will meet the following requirements: (i) modular and applicable for many unique capture devices, (ii) capable of interfacing with a variety of measurement tools, and (iii) easy to adopt and fabricate. Here, the proposed platform development is outlined with specific configurations and validation experiments highlighted. The strengths and weaknesses of this platform are discussed alongside experimental data acquired using said platform.

3 Materials and Methods

3.1 Resin and prepolymer solution preparation

Commercial ABS-like resin (Anycubic and Elegoo) was used for printing structural components for the air tunnel. Miicraft BV-002a black resin (Creative CADworks) was used for PDMS mold fabrication. Monocure rapid clear resin was used for some structural components as well as capture device fabrication. Two different in-house formulations were used for capture device fabrication. The first termed AN09 consisted of the following; 98.5% (w/w) polyethylene glycol diacrylate (PEGDA) 250 average molecular weight as the monomer, 0.5% (w/w) Diphenyl(2,4,6-trimethylbenzoyl)phosphine oxide (TPO) and 0.8% (w/w) Isopropylthioxanthone (ITX) was stirred at room temperature overnight. The second formulation termed AA09 consisted of 10% (w/w) Acrylic Acid (AA), 0.5% TPO, 0.8% ITX and 88.5% PEGDA stirred together at room temperature overnight. Resins were all stored in light impermeable containers.

3.2 3D printer operation

3.2.1 FDM printing

Fused deposition modelling (FDM) printing was conducted on a modified ender 5 pro printer (Creality), using a Dragonfly hot end (Phaetus) and dual drive extruder (Microswiss) onto a PEI build plate (TwoTrees). Prints were executed at varying temperatures, speeds and cooling settings depending on the resolution required and the material used. Materials explored include: TPU 95A, PETG, ABS, ASA, PLA, PLA+ and PA6-GF Nylon. Multi-material prints were achieved by pausing prints, swapping materials and settings and continuing the print at the layer it paused to ensure solid adhesion.

3.2.2 LCD MSLA printing

LCD MSLA printing was carried out on both the Elegoo Mars and Elegoo Mars Pro printers. For the Miicraft BV-002a resin with 20 μm layer thickness, 3s layer exposure times were used with a 40s base exposure. For ABS-like resin with 50 μm layer thickness, 4s layer exposures were used with a 30s base exposure.

3.2.3 DLP printing

DLP printing was carried out on both Miicraft hyper 80 (385 nm & 405 nm) printers and Asiga Max (385 nm). AN09 and AA09 were printed on the Miicraft printers with 20 μm layers at a layer exposure time of 1s and 2 base layers of 4s. AN09 was printed on the Asiga printer with 20 μm layers at a layer exposure time of 1s and a base exposure time of 10s.

3.3 Post processing of printed material

Resin printed parts underwent various post processing depending on their purpose and material. Typically the parts were rinsed in isopropanol (IPA) before being blown dry with compressed air and then subjected to a UV post cure for up to 4 minutes. Large parts with no sensitive details were washed in IPA while sonicated for up to 15 minutes prior to drying. Sensitive components were rinsed in IPA on a orbital shaker while protected from light for up to 20 hours to prevent the destruction of delicate structures. Parts with internal geometries where resin could be left behind were cleaned by using a syringe to force IPA through the internal cavities and then submerged in IPA to remove bubbles. BV-002a resin was additionally baked at 60 Celsius overnight after UV curing and before PDMS molding.

3.3.1 Surface treatments

the surfaces of prints were modified in a number of ways to achieve the desired surface features or properties. ASA and ABS-based FDM prints were exposed to acetone vapor to remove layer lines and create a smooth surface. Resin printed components which required a hydrophobic surface were either dipped into Rain-X and agitated for 5s and then blown dry or underwent microcontact printing through PDMS conformal contact. To create a temporary hydrophilic surface oxygen plasma treatment was used. For a longer lasting hydrophilic surface, tunable ratios of P100 and X100 (Joninn) were used.

3.4 Air tunnel

3.4.1 Hermetic seal evaluation

The air tunnel was subjected to airflow from pressurized air, and an outlet on the opposite end of the tunnel was left open. All other openings and vents are sealed shut. The entire CACD platform is then submerged in a shallow tank of water to observe the bubbling of air from seams which are not hermetically sealed. Alternatively, without the presence of a submersion tank, the tunnel was

completely sealed except for the air input, and soapy water was sprayed onto the seams and threads in question to see where soap bubbles formed.

3.4.2 Particle measurement

Earlier air tunnel versions used a HT-9600 air quality detector capable of measuring temperature, humidity, PM0.3, PM2.5 and PM10. It used a optoelectronic type sensor with an active sample pumping system and a laser diode light source. It collected data for 120 seconds before providing an average for the sample period.

Validation particle measurements outside of the test platform were conducted using the CO2 Click Model E Air quality monitoring sensor. This device uses a particulate matter measurement module from Piera Systems (IPS-7100).

The final iteration of the air tunnel uses a DualPDA (phase doppler anemometry) system from Dantec Dynamics, capable of measuring the distribution of particle sizes as well as their respective velocities in real time. The lasers of the PDA pass through the optically clear walls of the air tunnel to measure particles before and after the ACD. The PDA measurement system can be used on all types of particles, but the present data obtained by the PDA only utilizes DEHS particles.

3.4.3 Pressure measurement

Pressure measurement in the final wind tunnel iteration was conducted using MLH500PSG01B sensors from Honeywell. These are industrial 0 psi - 500 psi sensors with a sealed gage pressure reference for accurate quantification. They interface with the CACD platform using 1/4 inch NPT threads at symmetrical locations before and after the ACD. The output is in the range of 4-16 mA and interpreted to a pressure value by calibrated LabVIEW software (National Instruments).

3.4.4 Air speed and regulation

The first anemometer tested was a BT-846A sensor capable of measuring air speed ranging from 0.0 to 45.0 m/s as well as temperature. This anemometer was removed from its commercial construction and inserted into a custom housing manufactured using FDM printing from PLA for interfacing with the test platform (Figure.9).

Later iterations of the CACD platform used the VelociCalc Air Velocity Meter 9515 (TSI) with a velocity range of 0.0 - 20.0 m/s. This is a hot wire anemometer which measures the air speed through the amount of current needed to hold the wire at a specific temperature. Higher airflow will cool the wire faster and thus require a higher current. This type of anemometer is more reliable

and less affected by turbulence than vane anemometers.

The flow of air was controlled using the HFM-200 Mass Flow Controller for Low Flow (Teledyne) capable of 0.0 - 25.0 standard liters per minute (sLm). This controller forces air through at a given rate up until a maximum pressure of 500 psi. This is preferred to a pressure controller as we can then know the exact airspeed within the ACD. This controller interfaces with the LabView software mentioned earlier and connects to the CACD platform using Swagelok fittings.

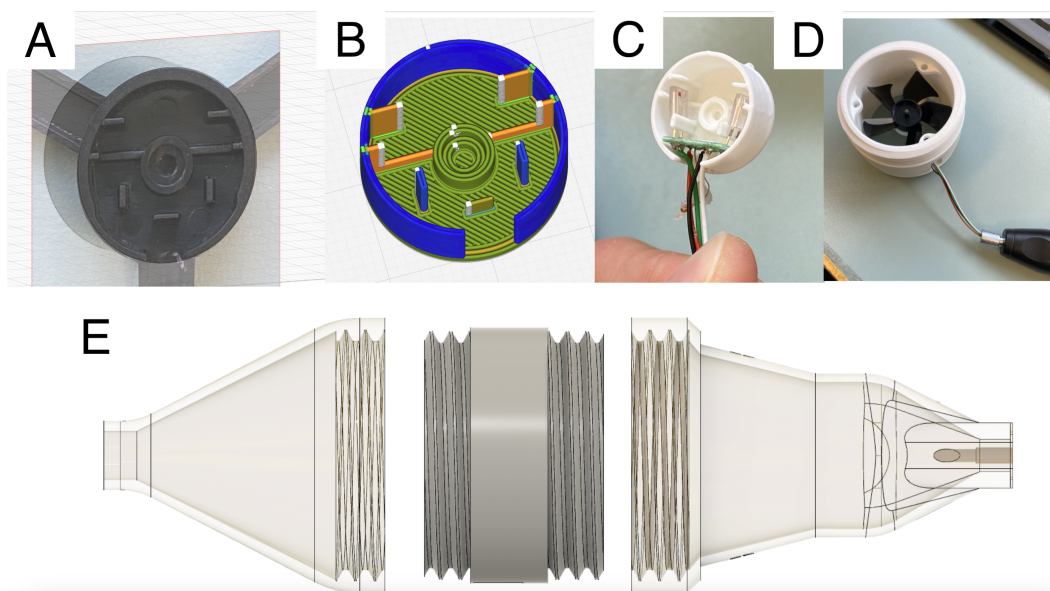


Figure 9: Design and fabrication of custom anemometer housing. a) Imported image of original vane anemometer housing. b) 3D model prepared for FDM printing via slicing software. c) FDM 3D printed construct fitting with optical sensor. d) Assembled anemometer unit with vane in place. e) Side view of entire anemometer component assembly.

3.4.5 Aerosol particle generation

The TurboBOY SX aerosolizer (Pari technologies) was used for qualitative measurements of particle capture with earlier vacuum powered iterations of the CACD platform. $3\ \mu\text{m}$ monodisperse polystyrene beads (polysciences) were diluted in PBS or Tween 0.1% before aerosolization and capture. Capture was validated through the presence of polystyrene beads on the capture substrate.

Quantitative measurements were carried out using a ATM 221 (TOPAS) aerosolizer operating on compressed air. This aerosolizer generates polydisperse aerosols with mainly submicron size, but that can be adjusted depending on the solution used. Di-Ethyl-Hexyl-Sebacat (DEHS) was utilized as the aerosolized substrate in the quantitative measurements due to its clarity, non-toxicity and residue free slow evaporation. This is ideal for the CACD platform as it means that the contamination of the interior will remain at a minimum from experiment to experiment.

Aerosol particle drying was conducted utilizing a 50 cm long drying column filled with anhydrous calcium sulfate. Aerosolized polystyrene particles were subjected to drying prior to entering the CACD to reduce them to particle nucleus size. DEHS generated aerosols were not subjected to drying as in this configuration the entire distribution of particle sizes is of interest.

3.5 Macro photography

Macro images were obtained using a Sony A7RIII camera with a FE 90 mm F2.8 Macro G OSS lens. Additional magnification was obtained using macro extension tube to reduce the minimum focal distance of the camera. Pixel shift imaging was also implemented to allow for higher resolution imaging. Sony Imaging edge software was used for remote control of the camera during focus stacking image acquisition. These image slices were then reconstructed into complete images using CombineZP. Raw images were processed through Adobe Lightroom for formatting.

3.6 Microscope imaging

Imaging was conducted on a Nikon Ti2 confocal microscope using NIS-Elements advanced research software. Image post processing was done using Fiji.

4 Results

4.1 CACD platform development

4.1.1 Design iterations, choices and rationale

The purpose of the characterization of aerosol capture devices (CACD) platform was to deliver aerosol laden air to an ACD in a consistent method such that the capture efficacy of that device could be evaluated. Multiple iterations and improvements were made as different solutions to challenges facing the platform were explored.

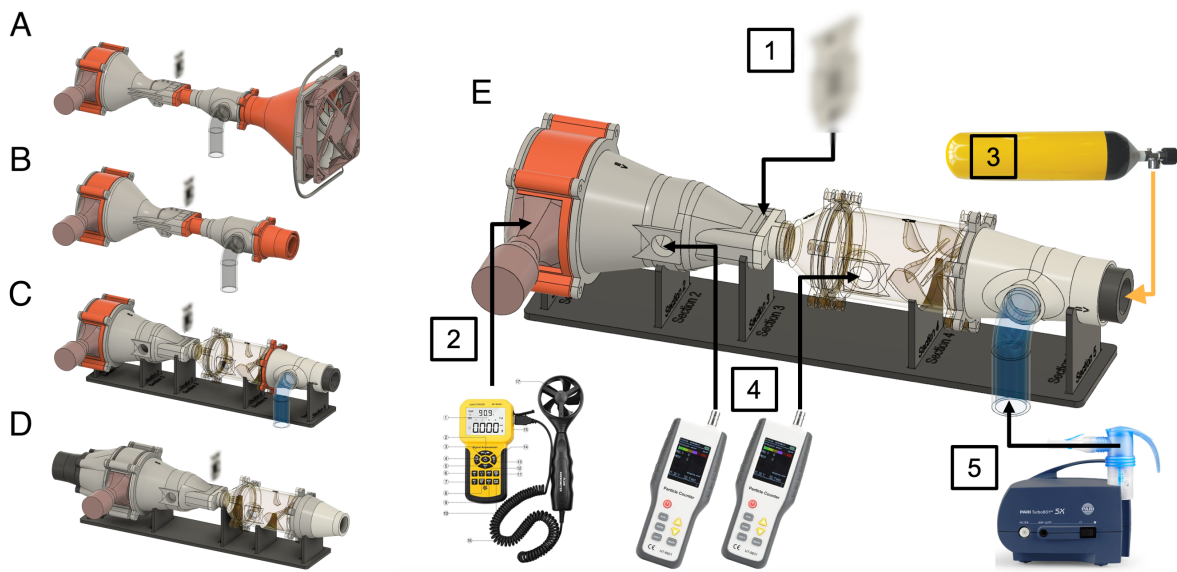


Figure 10: CACD platform versions 1-4. a) CACD platform version 1. b) CACD platform version 2. c) CACD platform version 3. d) CACD platform version 4. e) Schematic of peripherals for CACD platform 3. (1: ACD insertion slot. 2: Vane anemometer. 3: Pressurized air. 4: HT-9600 particle counter. 5: Turboboy aerosolizer.)

Initial versions 1-4 of the platform are shown in Figure.10 A-D with individual components displayed in Figure.10E. Versions 1 & 2 did not implement any particle measurement apart from the tested ACD and relied on radial and axial fans for their airflow. Versions 3 & 4 used HT-9600 particle counters before and after the capture device to quantify particles into $0.3\mu\text{m}$, $2.5\mu\text{m}$, and $10\mu\text{m}$ bins. The following features were present in iterations 1-4: A commercial anemometer system within either its original housing or the redesigned housing described in the methods section. The Turboboy aerosolizer for particle generation in either a lateral or medial configuration. The addition of vortex fins immediately prior to the capture device within the airflow to promote mixing.

Over these iterations, fundamental weaknesses of platform versions 1-4 were identified and resolved in version 5. Air consistently leaked out of the platform under pressure from the joints between tunnel sections and the interfaces with peripheral measurement devices. Particulate matter was found along the walls of the platform during aerosol tests, likely due to two causes. Primarily due to the aerosolizer used, which even in a medial configuration produced aerosol particles with a high exit velocity and large enough size to impact upon the walls of the platform. Second, the internal surface of the channel was rough due to its fabrication method relying on FDM 3D printing with a z resolution of $\sim 200 \mu m$. Finally the sensors used were found to be unreliable in this configuration due to the pressures involved in the CACD platform.

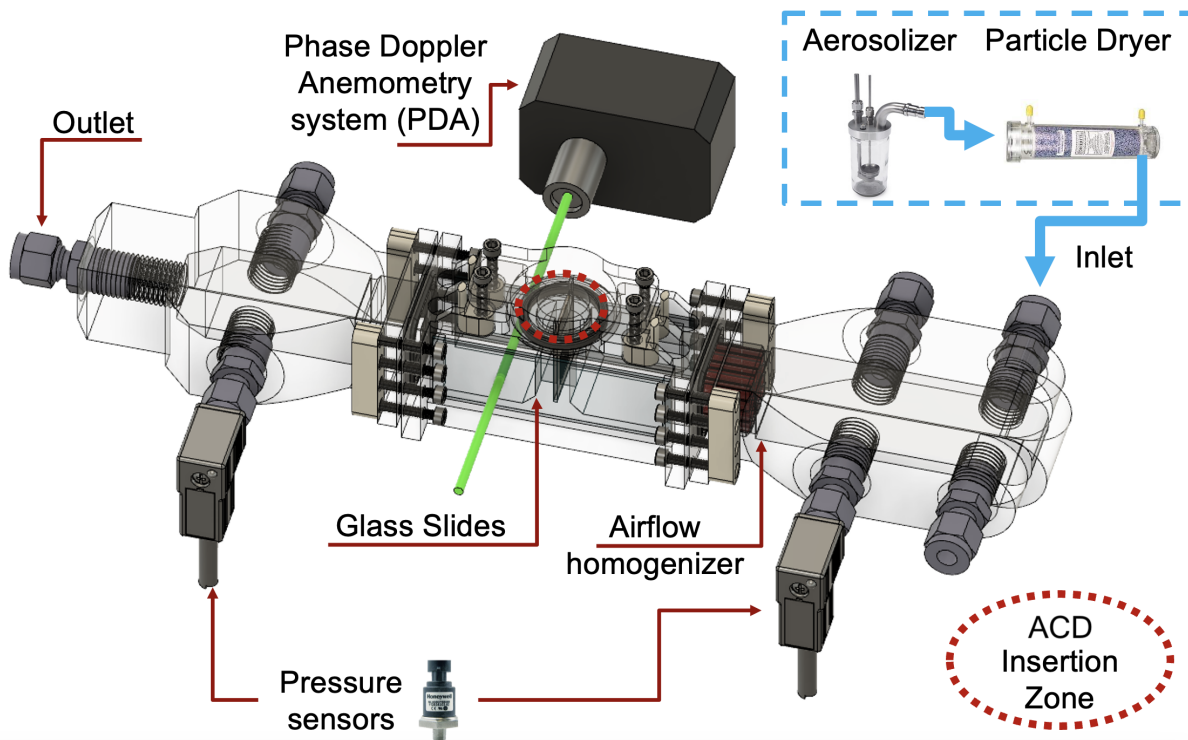


Figure 11: CACD platform version 5 depicted with input, output modules and the PDA compatible quantification core clamped together utilizing gaskets for sealing. The quantification core includes glass walls to allow for PDA measurements. The capture device insertion zone is highlighted in the middle of the platform. Particles undergo aerosolization and drying prior to injection into the clean airstream and entering the capture area.

The most recent iteration of the CACD platform (version 5) shown in Figure.11 was built upon the failures of the previous iterations. It utilized a phase doppler anemometry system (PDA) shown in Figure.13C for accurate determination of particle size and velocity immediately prior and following the capture device. This system illuminates the sample from the outside of the CACD platform on one side and measures the scattering using a sensor on the opposite side, removing

the sensor from the inside of the CACD platform. To take advantage of this system optically clear walls were necessary and both glass slides and acrylic walls performed well. However, due to the pressures which could build up within the CACD platform, acrylic was chosen as the window material due to the danger of projectile glass shards upon a catastrophic pressure release.

This platform iteration implemented a hot wire anemometer which constitutes an advancement over the vane anemometers in the previous versions. The addition of industrial pressure sensors previously lacking from the CACD platform enabled the quantification of pressure drop across the capture device. While the version 5 CACD platform retained an airflow homogenizer prior to the capture device, the rest of the aerosol generation pathway was replaced. A standardized jet aerosolizer was used instead of the Turboboy aerosolizer, and an additional particle drying step was implemented to reduce particle size variation. An understated but important aspect of the version 5 CACD platform is its utilization of standard NPT-1/4 threads for connecting peripherals which allows other standard measurement tools and airflow sources to be used easily.

Initially a PDMS soft sleeve was designed which could conform to the minute variations in capture device dimensions and provide an airtight seal. The mold was printed in both ABS-like and PEGDA-based resins (Figure.12B), but suffered from incomplete PDMS curing due to crosslinking inactivation (Figure.12C). This was replaced with a friction fit which satisfied the needs of the ACD insertion slit and improved the accessibility of the capture device within the wind tunnel (Figure.13 A&B).

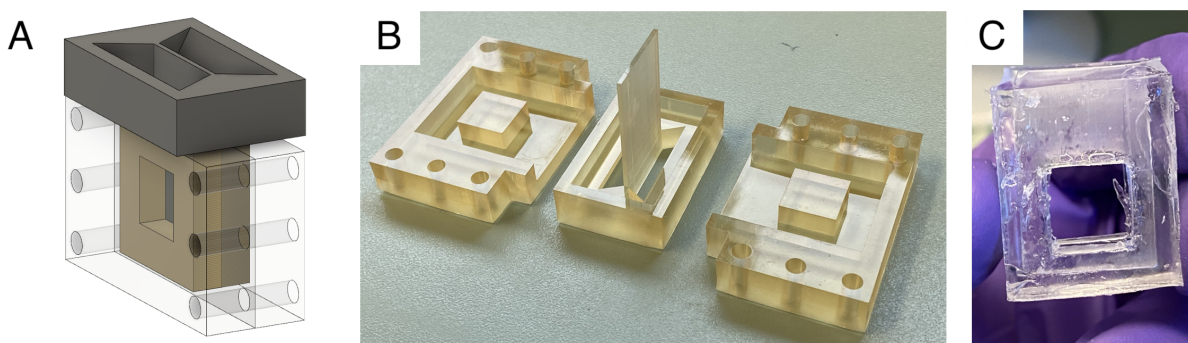


Figure 12: The making of a PDMS sleeve for hermetic sealing of a capture device within the characterization platform. a) The CAD render of the mold design. b) Printed components of mold in ABS-like resin. c) The final extracted PDMS construct after curing.

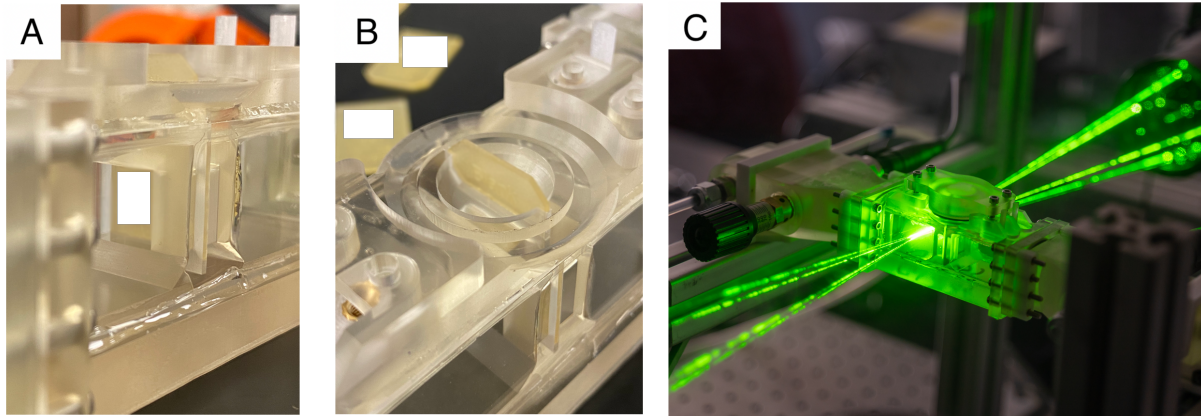


Figure 13: Capture device situated within the characterization platform and visuals of PDA measurement. a) View through the optically clear windows to see the capture area of the ACD. b) Top of the detection zone visible with protruding ACD (sealing lid and gasket removed). c) Active PDA measuring aerosol particles during an experiment.

4.1.2 Airflow sources

Several devices were tested for their ability to provide stable and clean air flow to the air tunnel and capture device. A standard Noctua 120 mm axial fan was tested as a economical and commercially available option, controlled and powered by a custom Arduino configuration (Figure.10A). However, axial fans of this caliber do not possess sufficiently high static pressure output to effectively force air through the CACD platform with the capture device in place.

Radial fans have significantly higher static pressures than axial fans and so a 3/4 horsepower powerful radial blower was adapted to power the air tunnel (Figure.10B). This air source had sufficient power to force air through the platform, but lacked fine control as it only had two speed settings. Additionally, when running for extended periods of time the blower fan would heat up the air it forced through the wind tunnel as can be seen in Figure.14B. The heating effect was even more significant when a high resistance insert was introduced into the airflow.

Another option for delivering air flow to the capture device is through the use of a vacuum at the exit of the air tunnel, allowing atmospheric pressure to push air through the device (Figure.10D). This has the added advantage of removing any turbulence prior to the device which fans may cause. However, the air speed measurements obtained from a vacuum configuration of version 4 CACD platform shown in Figure.14A demonstrated a variation of up to 17% over two minutes. This sort of variability is wholly unsuited for the precise characterization of the capture efficiency at different air speeds.

CACD platform version 5 utilized a HFM-200 Mass Flow Controller for Low Flow to deliver compressed air precisely, solving the previous issues of inconsistent flow and temperature varia-

tion.

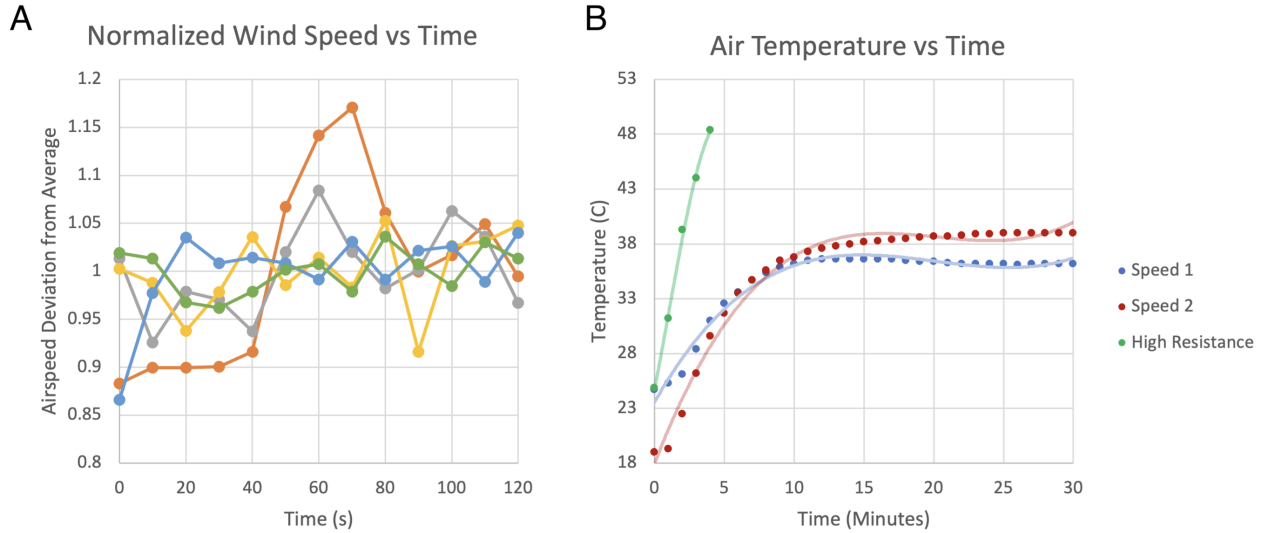


Figure 14: Air speed and temperature variation in the CACD platform version 3. a) Mean normalized wind speed over two minute sample period for 5 capture devices from different manufacturing runs. b) Temperature within the CACD platform over time with radial blower at low speed, high speed and with high flow resistance.

4.1.3 Material selection

The material surface properties of the CACD platform were of crucial consideration as they could heavily impact the deposition and flow of aerosols through the platform. The initial versions 1-4 utilized mainly FDM printed parts made with PLA and PETG polymers due to their availability and ease of printing. These components suffered from air leakage and surface aerosol accumulation as a consequence of the rough surfaces produced by FDM printing. To fix the air leakage, gaskets were designed and printed in flexible thermoplastic poly-urethane (TPU) to adjust for the surface variability of parts. Integrated gaskets were also attempted using multi-material printing of PETG and TPU shown in Figure.15 A&B. PLA and TPU multi-material printing was also explored but not pursued as they do not form as strong a bond as PETG and TPU. The integrated gaskets did not solve the issue as they still had the surface imperfections characteristic of FDM parts, and the TPU was not flexible enough to fill the gaps. Commercial rubber gaskets clamped between resin printed component interfaces solved these leakage issues in version 5 of the CACD platform.

Instead of using FDM printing for the structural components, resin printing was explored as it produces smooth surface finishes with $\sim 20 \mu m$ z resolution. Initially the PEGDA-based AN09 resin was tested, but due to its high price and brittleness it was not pursued further. Commercial

ABS-like resin was optimized for the final construction of the version 5 CACD platform. Multiple standard industrial thread designs (Ansi unified thread, ISO metric thread, ISO pipe threads, BSP pipe thread, DIN pipe thread, NPT thread) were tested in Figure.15 C&D to find the most suitable for this particular application. Producing functional NPT 1/4 threads allows the V5 platform to interface with standard peripheral measurement and airflow sources as well as exchange them at a later date. The threaded interfaces aided by teflon plumbers tape provided a robust and airtight seal.

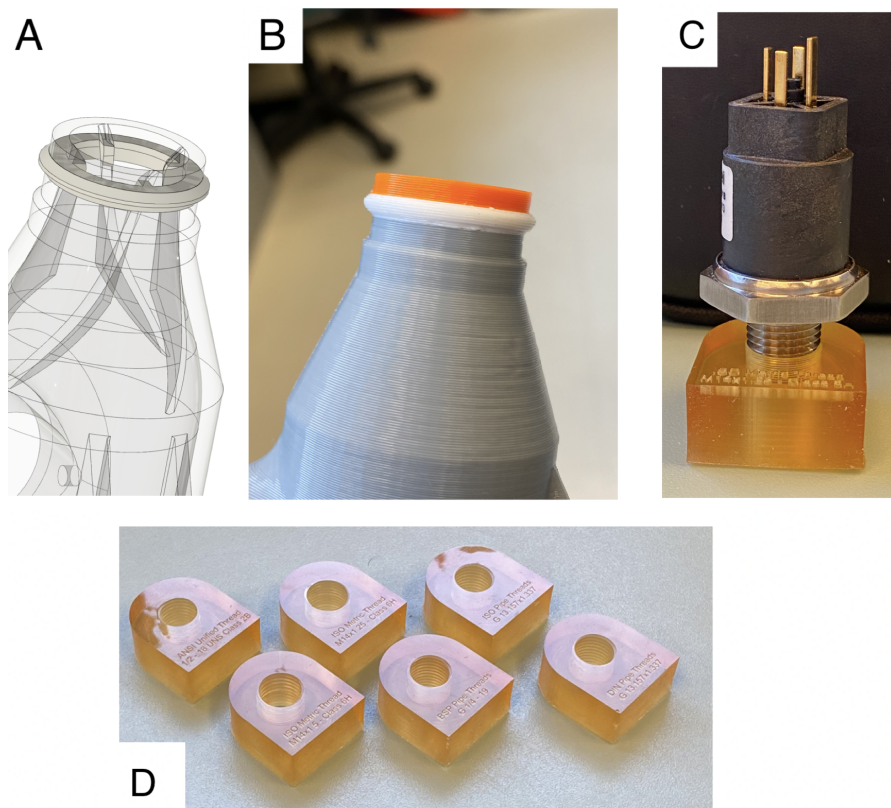


Figure 15: Integrated TPU gaskets, thread fitting and optimization. a) CAD design of the multi-material integrated flexible TPU gasket shown in white. b) FDM print using grey PETG, white TPU, and orange PETG. c) Correctly fitted pressure sensor hermetically threaded into material. d) 6 Different standard threads printed in PEGDA resin.

Within the optimization process, two different resins were tested for component fabrication, monocure and a PEGDA-based resin. The effect that base exposure time and layer exposure time had on the correct formation of complex internal structures and Z dimensional accuracy is illustrated in Figure. 16. Generally as the layer exposure time increased, the resolving capability decreased for both PEGDA and monocure resins, with PEGDA showing overall superior final products. The layer exposure time and base exposure time were both not found to have significant

impacts on the Z dimensional accuracy of the parts. Small feature analysis showed that any base cure time over 2.5 seconds resulted in occluded through pores below $500\ \mu m$. Finally however an alternative commercial ABS-like resin was utilized for the majority of structural components due to its price, lack of post print warping and lack of variability.

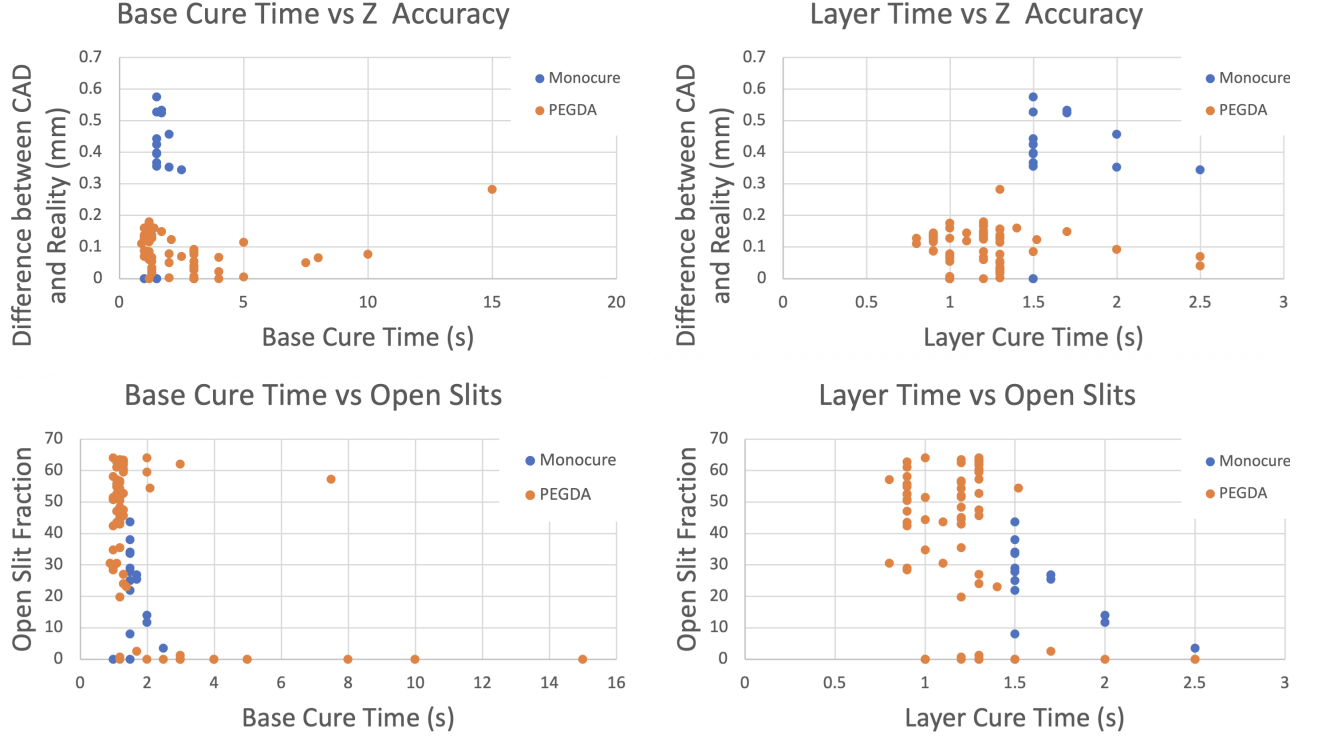


Figure 16: Monocure resin compared to PEGDA resin based on the Z-accuracy (Z-acc) and performance on small slit features (open slit fraction OSF). Comparison conducted for both base exposure time (BET) and layer exposure time (LET). (From left to right: OSF vs. BET, Z-acc vs. BET, OSF vs. LET, Z-acc vs. LET. Orange = PEGDA, Blue = Monocure.)

4.1.4 Sensor selection and validation

The HT-9600 particle counter was chosen due to its ability to measure temperature humidity and classifying particles into $0.3\ \mu m$, $2.5\ \mu m$, and $10\ \mu m$ bins. It uses integrated active pumping to sample air for analysis during a 2 minute data collection period. This device was used in versions 3&4 of the CACD platform, inserted into the airstream through holes in the side wall. Comparing the empty platform to an ACD present yielded the particle measurements shown in Figure.17. The parafilm used to seal these openings with the particle counters was not sufficient to provide a hermetic seal under pressurized conditions.

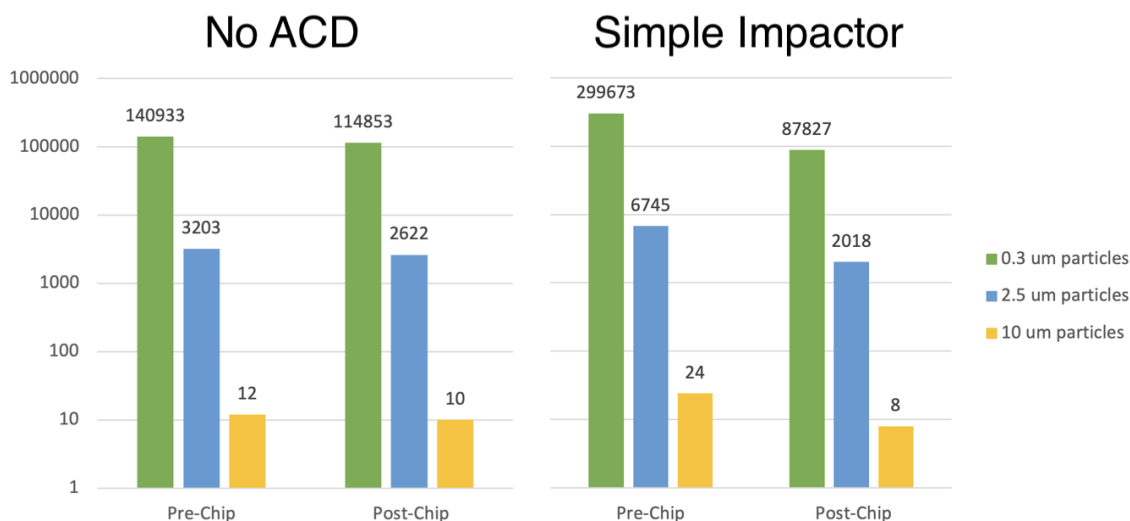


Figure 17: Particle count measurements using the HT-9600 before and after the capture zone for both a impaction capture device and a blank. Measurements were taken for 0.3, 2.5, and 10 μm particles.

The HT-9600 particle counter was compared with the reliable and higher quality CO2 Model E air quality sensor. However the CO2 Model E cannot be fitted to the CACD platform as it lacks the appropriate inlet system. Instead it was used for the validation of the HT-9600.

The performance of the two systems is shown in Figure.18 for sampling in the offices, lab space, biosafety hood, outdoors and also when subjected to human exhalate. The two systems show varying results for the majority of sampling sites, with a difference of up to 2 orders of magnitude between them. The Model E recorded a value of 0 for PM10 at all sites except breath while the HT-9600 measured between 3-7 10 μm particles/liter again except for breath. The difference between PM0.3, PM2.5 and PM10 measurements for the HT-9600 was consistent from sample to sample, with only the overall abundance able to differentiate. The Model E demonstrated higher resolving ability as it recorded varying levels of particles at different sizes and locations.

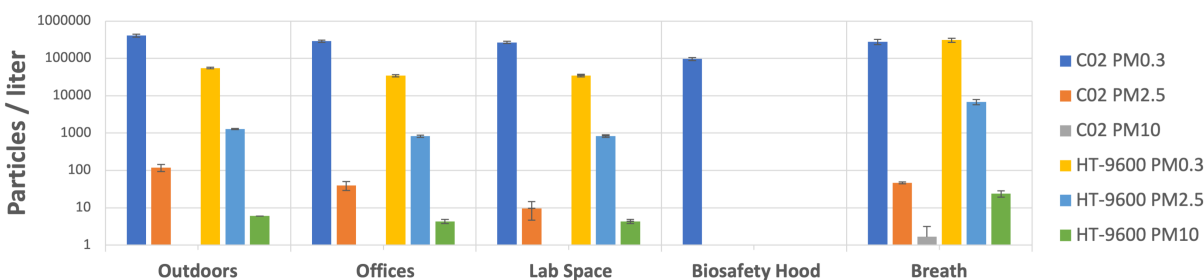


Figure 18: Comparison of CO2 Click Model E air quality sensor with the HT-9600 air quality sensor in the following environments: Outdoors, Offices, Lab space, Biosafety hood, Breath. (Std Dev error bars, n=3)

4.1.5 Performance of the CACD platform version 5

Building upon the observations and results of the previous platforms the version 5 CACD platform was designed to solve the challenges facing previous versions. Presented initially in section 4.1.1, the complete annotated design can be seen in Figure.11. The recommended operating parameters and specifications of the CACD platform are listed in Table 3 below as well as the potential sizes of ACDs it can accommodate.

Table 3: CACD platform (Version 5) specifications.

Metric	Platform specifications
Size	300 mm x 60 mm x 50 mm
Flow rate	1-100 L/min
Capture device size	Reconfigurable up to 2 cm x 2 cm x 2 cm
Operating pressure	0-10 psi to avoid glass breakage
Particle measurement	PDA measures effectively 0.2 μm
Pressure measurement	0-10 psi dynamic range

Measurements obtained by the PDA in version 5 of the CACD platform are shown in Figure.19. The distribution of particles was measured before and after the capture zone for a blank sample, a simple flow restrictor and a impaction based ACD. The flow constrictor consists of a hole of known diameter and the impactor consists of an array of accelerating nozzles and impaction plates. The impactor was developed in the Juncker lab, and the capture rate and pressure drop have been predicted but have not been experimentally characterized prior to these experiments. The ACD's tested within this platform are solely for the sequestration of aerosols and do not contain integral particle measurement tools. The accumulated particles can be extracted from the ACD to establish the quantity of captured material. The blank measurement showed almost identical values across the capture zone, in-line with the expectation of slight particle loss to the walls. The flow restrictor showed higher variability but still a significant drop in all particle sizes. Both the flow restrictor and the impactor measured less than 5 particles per bin for sizes above 10 μm after the capture zone. The capture rate of the empty CACD varies from 0 up to ~ 0.8 due to low number of particles and similarity the between the front and back measurements. The flow restrictor shows a capture rate increasing with particle size reaching $\sim 40\%$ capture for particles 0-3 μm , and 90 % capture for $> 8.5\mu\text{m}$ particles. The classic impactor performed similarly to the flow restrictor, reaching 90 % capture for $> 7.9\mu\text{m}$ sized particles. However, it outperformed the flow restrictor at the lower end, with a capture rate of $\sim 60\%$ for particles 0-3 μm and then increasing the capture rate with the particle size.

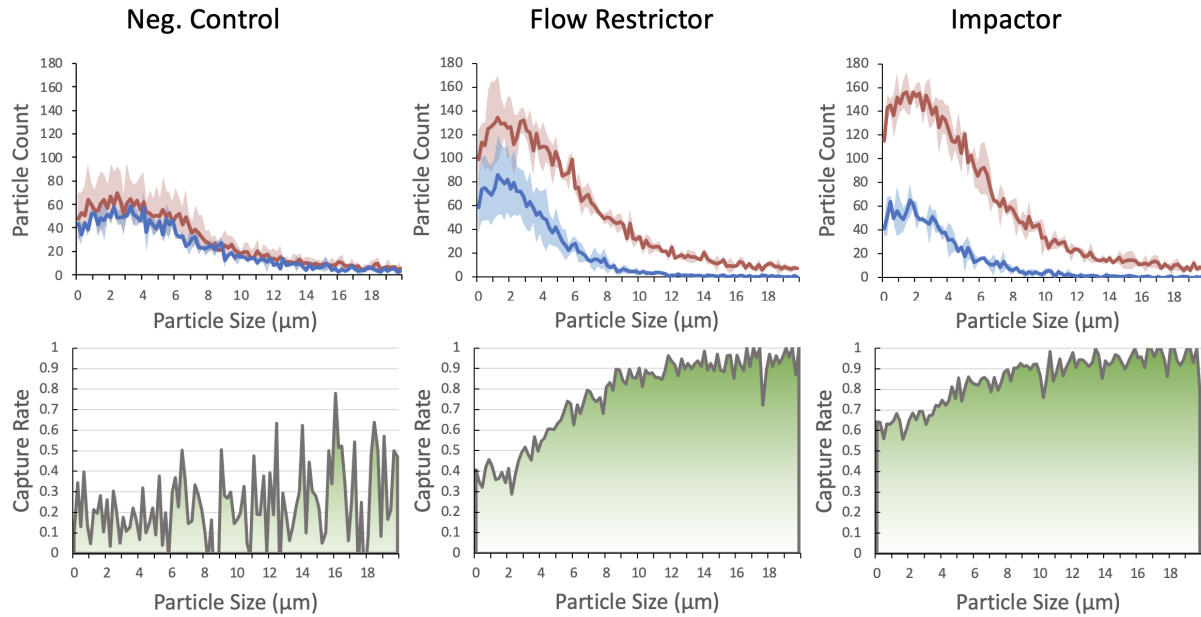


Figure 19: Particle size distributions before (Red) and after (Blue) the ACD for a flow restrictor, a in-house developed impactor and the negative control. Measurements were taken with the PDA system. Error range is 1 standard deviation, $n=3$)

The pressure sensors integrated in the CACD platform were utilized to measure the pressure at the inlet and outlet at flow rates of 20 l/min and 30 l/min (Figure.20). As the resistance level within the CACD platform is increased, the inlet pressure increased linearly but the outlet pressure was unchanged. This complies with theory as the outlet has an open path to atmospheric pressure, reducing the impact of the airflow pressure. The largest pressure drop measured was 800-1,000 Pa, well within the maximum expiratory pressure of human subjects (6k-9k Pa). The pressure sensors used were accurate up to 10 PSI, but due to the modular nature of the platform can easily be swapped for higher or lower threshold sensors.

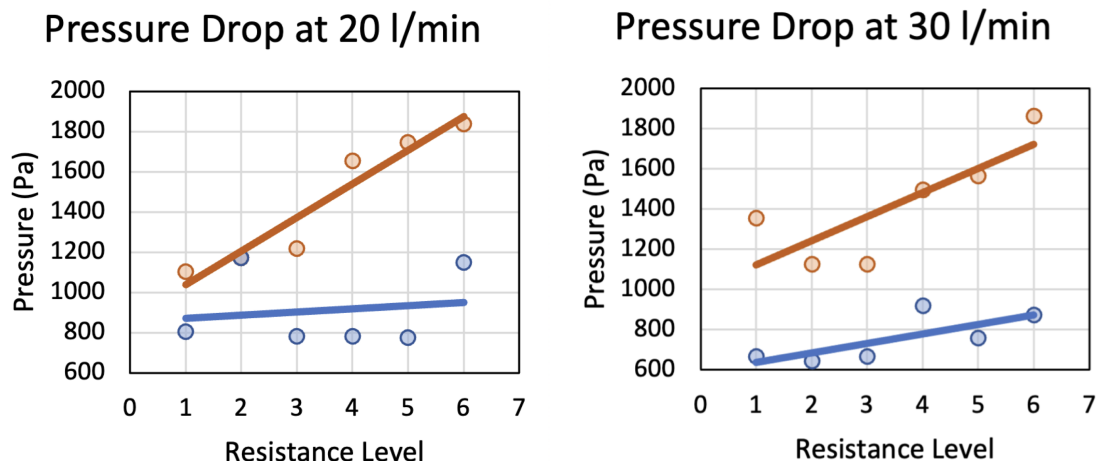


Figure 20: Pressure measurements before (Red) and after (Blue) the capture zone for multiple levels of flow restrictors. Higher resistance levels were achieved by forcing air through smaller gaps on the range of 80-200 μm .

Following this initial demonstration, unsatisfactory variability was noted for both the PDA and pressure measurements. The CV for PDA measurements within the 0.2-5 μm range without an ACD present was 0.083, but increased as far as 0.4 in the presence of an ACD. The measurements were not acquired in the exact same position due to the manipulation of the platform during device insertion and extraction. To remedy this, an automated XYZ stage was fitted to the PDA to reproducibly position the measurement instrument relative to the CACD platform. Additionally, the pressure measurements had a CV of 0.28 at the initially planned low sampling rate. This was rectified through the implementation of a large sample size acquisition protocol which yielded a CV of 0.11.

The CACD platform was designed for facile fabrication and modular assembly, allowing for utilization in different applications and resource limited environments. The majority of the construct is 3D printed with economic commercially available materials and a <300 USD printer. The results and characterization presented herein demonstrate the worth of this platform as a tool for the evaluation and comparison of ACDs.

5 Discussion

Here an evaluation platform for ACDs was developed through experiment guided iterative design. Unpacking the contents of aerosol particles can give insight into the infectiousness of an individual and answer questions about their metabolic state without the need for invasive sampling. To utilize this abundant sample set, ACDs must be developed which can sequester these particles for analysis efficiently and in high concentration.

5.1 Requirement of a custom platform

As discussed in the introduction, ACDs take advantage of different physical principles to sequester particles. These different capture mechanisms have different form factors, input/output requirements and even differing evaluation criteria. There are no standardized evaluation tools for novel ACDs such as the one we developed, therefore, a custom characterization platform was required. Depending on the device to be characterized, a test platform may have to accommodate large air-flow rates upwards of 100 l/min or precisely control smaller than 1 l/min flows. Some devices may specifically target capturing viable aerosols or submicron particles, each of which would require specialized evaluation techniques and equipment which may limit the breadth of analysis that a particular configuration can provide. Previous papers introducing novel capture devices often outline but do not emphasize the evaluation platforms associated with their devices, but they are important to consider alongside the actual device.

The results from the earlier iterations of the CACD platform demonstrated the importance of robust characterization. If the evaluation metric is unreliable, the results will grossly misrepresent the performance of the device in question. The ability to evaluate fairly and accurately an objective metric is instrumental to engineering and improving any device. This is especially important in our situation wherein the device and its evaluation are both novel, but have to be quantified and compared to existing devices in the field.

5.2 Advantages and challenges of current approach

The CACD platform introduced in this thesis has a number of benefits due to its flexibility and ease of fabrication and assembly. However, some of those same design choices are also the causes of its limitations.

The CACD platform was designed as a modular system wherein different components and units can be attached to serve specific functions. This ideology was carried throughout the design, the interfaces between the inlet assembly, the quantification core and the outlet assembly have

identical attachment and sealing features. The standardized NPT threads used on the inlet and outlet assemblies allow the connection of many different brands and styles of pressure sensors, relief valves, air inlets and outlets as well as aerosol supplies or any other future instrumentation. Adding all the inlets together into an assembly removes the need for external valving and mixing units as interfacial injection can be used to mix different airflows, and separate flow controllers can be fed into each of the different inlets in the assembly. The form factor of the platform is one of the overlooked but practically beneficial features which allows easy integration of the platform with other instruments which may not necessarily be as mobile. One such instrument is the PDA, a central component around which the V5 platform was built. Although the quantification core of the platform was designed to work with a PDA instrument, due to the modularity of the design, a different core section could be swapped in to accommodate other particle detection methods. Additionally, as the CACD platform was designed for 3D printing, many modern labs can tweak modules of this design for their own needs, and manufacture their own versions of the platform.

However, the design of the quantification core and the overall modular platform limit the applications of this configuration of the CACD platform. Since the PDA requires optically clear sidewalls for its laser to shine through, the walls of the core consist of glass or acrylic. These walls can only handle pressure safely up to 10 PSI, multiple times during testing and development catastrophic failures occurred with the internal pressure shattering the glass walls. As a consequence of this, pressure relief valves were fitted to the inlet assembly to prevent catastrophic depressurization. The core is also configured for a aerosol particle devices through which aerosol laden air passed directly through. Capture devices using complex airflow paths such as centrifugal flow or classic impingers may not work with this CACD platform unless the core is modified to suit those applications. Due to the small size of the CACD platform, extensive high concentration aerosolization resulted in particle agglomeration and the wetting of the walls within the quantification area. This would only occur after continuous aerosolization for 30 minutes, and was cleared by flushing clean dry air through the platform for 30 minutes. Normal operation of the platform consists of short bursts of high concentration aerosolization on the range of 0-5 minutes followed by flushing with dry clean air. This issue is not expected with low aerosol concentration tests.

The initial measurements obtained from the pressure system and the PDA regarding a simple impaction-based ACD varied significantly more than expected under differing conditions. The CV for initial pressure measurements was 0.28 with large variation between measurements of the same flow configuration. This was due to the small sample size and the inherent noise of the pressure sensor, with the implementation of a rapid (N=100) acquisition protocol reducing the CV to 0.11. The variation of the PDA measurements was unidirectional, with measurements in front of the

ACD relatively constant with a CV of 0.07 while measurements after the ACD varied significantly with a CV of 0.4. This was likely caused by two main factors; the number of particles drastically reduced after the ACD results in much larger variation in measurements specifically in the sparse larger particle ranges. The second cause of this variation is the movement of the CACD platform relative to the PDA during ACD insertion and extraction. This causes the measurement to occur at a slightly different site in the airflow with each device. To rectify this, an XYZ motion system was implemented to reproducibly position the PDA relative to the CACD platform with precision. Further validation of the CACD accuracy is required through characterization of ACDs with known capture rates to corroborate the PDA measurements.

5.3 Comparison of particle detection methods

Quantifying airborne particle sizes and counts is integral to determining the performance of an ACD. As such, the specific method used for this quantification has to be sensitive, operate consistently under different conditions and not disturb the performance of the capture device in any way. Over the development of the CACD platform, two particle detection methods were evaluated for the above requirements with a third used as validation.

Initial iterations used the HT-9600 optical particle counter, which draws air in through a tube placed into the sample air stream. While initially the HT-9600 showed promise, several flaws appeared as tests progressed. The HT-9600 showed a clear variation with the airspeed in the CACD platform, likely due to the active sampling mechanism, which was not suited for sampling from pressurized environments or air streams. Comparison with the CO2 Click Model E sensor highlighted the inadequacy of the HT-9600 as it was unable to differentiate between different sampling locations. While the HT-9600 claims to measure 3 different bins of particle sizes, it scaled all three bins up and down together rather than differentially to reflect the true particle size distribution. This was made abundantly clear in Figure.18 where the Model E sensor differentiated between breath, office and biosafety hood samples, while the HT-9600 maintained the same ratio of different particles simply scaled up or down.

As the entire CACD platform evolved to handle higher pressures and the precise control of airflow required, an appropriate particle measurement system was chosen in the form of a PDA. The PDA utilizes lasers to measure particle size distribution, and as such does not require any direct interaction with the sample itself or even the airflow. Additionally as the entire PDA is physically separate from the CACD platform, we found no pressure or air speed related effects on the particle distribution.

5.4 Comparison to existing evaluation platforms

The presented CACD platform falls within the requirements of other platforms presented in the literature. The two platforms discussed in the introduction used 1 L/min and 14 L/min of airflow, well within the capabilities of the CACD platform. They both utilize particle drying to control the size of volatile particles and precision air flow regulation to ensure constant flow. Pressure measurements are not standard in these platforms and are usually only implemented when the pressure drop of a device is relevant to its function. The integration of pressure sensors into the CACD platform allows for the measurement of this property of ACDs in place without complicated peripherals. One of the main features of the CACD over many existing test platforms is the usage of the PDA instead of active air samplers from the airstream. By removing any manipulation of the airstream, a more accurate capture performance of an ACD can be assessed. The majority of platforms recently introduced use such interfering sampling methods, likely resulting in slightly skewed ACD analysis. Additionally many platforms use extensive tubing to carry particle laden airflow from instruments to the capture site and back to measurement sites. Particle loss along tubing walls is a serious concern which can only be mitigated by localizing components as close as possible to each other. The CACD uses a single chamber for all the measurement components and ACD, removing the majority of the travel distance. Overall, the CACD platform resembles many of the existing characterization platforms with slight but consequential improvements in the instrumentation, the design and operation.

5.5 Design iteration and evolution

Each iteration in the design process for the CACD platform highlighted flaws and areas of improvement for the next version, leading to a consistently improving product. Often the predictions based on theory were not exactly representative of the actual results or failed to account for real world variables. One such example was the selection process for air supply system. While initially simple, this choice affected almost all the other aspects of the CACD platform. Initially fans were considered the easiest to setup, so radial and axial fans were both tested. Since the axial fans did not show sufficient static pressure for this application, a 3/4 horsepower radial fan was expected to solve the problem. However, the air exiting the radial fan was heated due to the high energy consumption of the fan, altering the aerosol particle conditions over the course of an experiment (Figure.14). Another consideration was whether to provide airflow through applying a pressure to the anterior of the platform or by applying reduced pressure to the posterior of the platform. Both approaches provide airflow, but the vacuum approach poses the threat of contaminating the

air stream with outside particles if any leaks are present. Furthermore, the vacuum approach limits the pressure differential across the ACD to atmospheric pressure while an over-pressure approach allows for more flexibility.

The exploration of different designs was restrained by the limits of the fabrication methods used, mainly FDM and LCD 3D printing. While both of these methods allow for the manufacturing of previously impossible structures, they suffer from surface imperfections and the inability to print in thin air. For the first 4 iterations, 3D printed custom TPU gaskets were tested both as integral features of the components and as stand-alone gaskets. While 3D printing the gaskets allowed for custom shapes, and the integral gaskets were an attractive option, they all suffered from slight air leakage due to the surface imperfections. The version 5 CACD platform used commercial rubber O-rings to achieve the perfect hermetic seal necessary for precise measurements. Similarly the interface of the capture device with the CACD platform was initially concerning, and to solve this challenge an overly complicated and over-engineered solution was devised. A 3D printed negative mold was printed to produce a PDMS sleeve capable of stretching to accept the capture device in an airtight seal (Figure.12). However, the entire production process of this PDMS insert took multiple days and resulted in a component which had to be replaced every couple of tests and did not perform better than a tight friction fit between hard components. Throughout this entire iterative design process, interpreting the failure modes and understanding the limitations of the available tools lead to both novel innovation as well as simpler logical solutions. Extensive understanding of the theory and background has to guide design and fabrication for the final product to perform as well as possible, but to get through the initial phases sometimes it is necessary to simply test a prototype and then dissect why it did not work.

5.6 Future directions

This modular platform was envisioned as an evolving combination of modules and peripherals to characterize many different ACDs. Additional modules could be added in series or in parallel with the main axis of the CACD platform or attached to the inlet and outlet ports. Already planned but not incorporated were flow regime modules directly prior to the quantification core which would promote either turbulent or laminar air streams. Similarly, a mixing unit to ensure the uniform distribution of aerosol particles in the air stream was envisioned and designed but never fabricated. Alternative quantification cores able to implement multiple aerosol measurement devices would provide the ability to further validate the platform. Additionally, further thorough validation is required with ACDs of known performance to calibrate the platform.

The CACD can also be repurposed for general aerosol analysis from its initial purpose of ACD

characterization. Aerosol particle behavior, evaporation and interactions can be probed within the quantification core through the PDA or other specialized instruments. Raman scattering has been used to investigate the composition of both in-motion aerosols and optically or electrodynamically trapped particles.[41] Specifically Raman scattering provides information on pharmaceutical aerosol composition and structure to improve lung deposition and respiratory cell drug uptakes.[32] Other instruments which could seamlessly integrate with the CACD include mass spectrometers, high speed cameras and

To explore other distributions of aerosol particles, varied aerosol generating configurations should be tested. Different aerosolizers and different fluids can result in vastly different particle distributions and behavior. Implementing viscoelastic fluids similar to mucus could provide valuable insight into the interaction of biologically relevant fluids with ACD's. Finally the platform should be adapted to fit other devices therefore providing a uniform platform for their even comparison. The platform is easily adaptable to the comparison of surgical, N95 and other fabric-based filtration devices in light of the recent Sars-Cov-2-2019 pandemic.

6 Conclusion

In summary, presented here is the design, optimization, fabrication and capabilities of an ACD characterization platform. Through iterative design and testing, challenges facing the instrumentation and airflow were identified and solved. Different fabrication methods, airflow sources and measurement devices were explored and compared to select those most suitable for this application. The 3D printed CACD platform presented herein allows aerosol laden airflow to pass through an ACD under precisely regulated conditions, with pressure and particle distributions measured before and after the ACD. The sensors used for both pressure and particle measurements were carefully selected for their sensitivity, minimal perturbation of ACD performance and compatibility with pressurized and aerosol laden environments. Applying the CACD platform to a real-world example of an uncharacterized impaction-based ACD demonstrated its utility in evaluating said device, but highlighted variability in the measurements. Following the initial demonstration, an automated movement stage was appended to the CACD platform to the aid the reproducibility of the PDA measurements. Additionally, an improved sampling protocol was implemented for the pressure measurements to improve the variability initially observed with small sample size measurements. Validating the CACD platform with ACDs of known performance is necessary for confidence in the quantitative output of the PDA and pressure sensors. Future improvements for the platform include airflow regime modulating adapters and alternative quantification core components for different ACDs and particle measurement systems. The platform is also to be applied to the measurement and analysis of common filtration-based breathing masks to compare their performance under varied conditions as well as other ACDs. The CACD platforms performance and flexibility make it a useful tool for the comparison and evaluation of ACDs in the rapidly evolving field of aerosol research.

References

- [1] S. Anand and Y. Mayya. Size distribution of virus laden droplets from expiratory ejecta of infected subjects. *Scientific reports*, 10(1):1–9, 2020.
- [2] M. P. Atkinson and L. M. Wein. Quantifying the routes of transmission for pandemic influenza. *Bulletin of mathematical biology*, 70:820–867, 2008.
- [3] J. E. Belizário, J. Faintuch, and M. G. Malpartida. Breath biopsy and discovery of exclusive volatile organic compounds for diagnosis of infectious diseases. *Frontiers in cellular and infection microbiology*, 10:564194, 2021.
- [4] L. Bonifait, R. Charlebois, A. Vimont, N. Turgeon, M. Veillette, Y. Longtin, J. Jean, and C. Duchaine. Detection and quantification of airborne norovirus during outbreaks in health-care facilities. *Clinical infectious diseases*, 61(3):299–304, 2015.
- [5] A. Bredberg, J. Gobom, A.-C. Almstrand, P. Larsson, K. Blennow, A.-C. Olin, and E. Mirgorodskaya. Exhaled endogenous particles contain lung proteins. *Clinical chemistry*, 58(2):431–440, 2012.
- [6] A. Bredberg, M. Josefson, A.-C. Almstrand, J. Lausmaa, P. Sjövall, A. Levinsson, P. Larsson, and A.-C. Olin. Comparison of exhaled endogenous particles from smokers and non-smokers using multivariate analysis. *Respiration*, 86(2):135–142, 2013.
- [7] P. R. Buseck and M. Pósfai. Airborne minerals and related aerosol particles: Effects on climate and the environment. *Proceedings of the National Academy of Sciences*, 96(7):3372–3379, 1999.
- [8] D. Y. Choi, K. J. Heo, J. Kang, E. J. An, S.-H. Jung, B. U. Lee, H. M. Lee, and J. H. Jung. Washable antimicrobial polyester/aluminum air filter with a high capture efficiency and low pressure drop. *Journal of hazardous materials*, 351:29–37, 2018.
- [9] J. Choi, J. S. Kang, S. C. Hong, G.-N. Bae, and J. H. Jung. A new method for the real-time quantification of airborne biological particles using a coupled inertial aerosol system with in situ fluorescence imaging. *Sensors and Actuators B: Chemical*, 244:635–641, 2017.
- [10] J. Choi, J. Lee, and J. H. Jung. Fully integrated optofluidic sers platform for real-time and continuous characterization of airborne microorganisms. *Biosensors and Bioelectronics*, 169:112611, 2020.

- [11] R. B. Couch, P. J. Gerone, T. R. Cate, W. R. Griffith, D. W. Alling, and V. Knight. Preparation and properties of a small-particle aerosol of coxsackie a21. *Proceedings of the Society for Experimental Biology and Medicine*, 118(3):818–822, 1965.
- [12] J. P. Crimaldi, A. C. True, K. G. Linden, M. T. Hernandez, L. T. Larson, and A. K. Pauls. Commercial toilets emit energetic and rapidly spreading aerosol plumes. *Scientific Reports*, 12(1):20493, 2022.
- [13] M. D. Davis, A. Montpetit, and J. Hunt. Exhaled breath condensate: an overview. *Immunology and Allergy Clinics*, 32(3):363–375, 2012.
- [14] D. Ehrenstein. How speaking creates droplets that may spread covid-19. *Physics*, 13:157, 2020.
- [15] J. Q. Feng, L.-S. Go, J. Calubayan, and R. Tomaska. Working mechanism and behavior of collision nebulizer. *Aerosol Science and Engineering*, 5(3):285–291, 2021.
- [16] F. T. Gucker and C. O’Konski. Electronic methods of counting aerosol particles. *Chemical reviews*, 44(2):373–388, 1949.
- [17] M. Hagbom, J. Nordgren, R. Nybom, K.-O. Hedlund, H. Wigzell, and L. Svensson. Ionizing air affects influenza virus infectivity and prevents airborne-transmission. *Scientific reports*, 5(1):11431, 2015.
- [18] C. W. Hinds. *Aerosol technology*. John Wiley & Sons, 2 edition, 1999.
- [19] I. Horváth, P. J. Barnes, S. Loukides, P. J. Sterk, M. Högman, A.-C. Olin, A. Amann, B. Antus, E. Baraldi, A. Bikov, et al. A european respiratory society technical standard: exhaled biomarkers in lung disease. *European Respiratory Journal*, 49(4), 2017.
- [20] I. Horváth, J. Hunt, P. J. Barnes, et al. Exhaled breath condensate: methodological recommendations and unresolved questions. *European Respiratory Journal*, 26(3):523–548, 2005.
- [21] J. A. Huffman, A. E. Perring, N. J. Savage, B. Clot, B. Crouzy, F. Tummon, O. Shoshanim, B. Damit, J. Schneider, V. Sivaprakasam, et al. Real-time sensing of bioaerosols: Review and current perspectives. *Aerosol Science and Technology*, 54(5):465–495, 2020.
- [22] E. Kaufman and I. B. Lamster. The diagnostic applications of saliva—a review. *Critical Reviews in oral biology & medicine*, 13(2):197–212, 2002.

- [23] L. Kenny, A. Thorpe, and P. Stacey. A collection of experimental data for aerosol monitoring cyclones. *Aerosol Science and Technology*, 51(10):1190–1200, 2017.
- [24] B. Keshavarz, E. C. Houze, J. R. Moore, M. R. Koerner, and G. H. McKinley. Ligament mediated fragmentation of viscoelastic liquids. *Physical review letters*, 117(15):154502, 2016.
- [25] S. Kooij, A. Astefanei, G. L. Corthals, and D. Bonn. Size distributions of droplets produced by ultrasonic nebulizers. *Scientific reports*, 9(1):6128, 2019.
- [26] S. M. Kreidenweis and A. Asa-Awuku. *5.13 - Aerosol Hygroscopicity: Particle Water Content and Its Role in Atmospheric Processes*. Elsevier, second edition edition, 2014.
- [27] P. Kubáň and F. Foret. Exhaled breath condensate: determination of non-volatile compounds and their potential for clinical diagnosis and monitoring. a review. *Analytica chimica acta*, 805:1–18, 2013.
- [28] P. Larsson, E. Mirgorodskaya, L. Samuelsson, B. Bake, A.-C. Almstrand, A. Bredberg, and A.-C. Olin. Surfactant protein a and albumin in particles in exhaled air. *Respiratory medicine*, 106(2):197–204, 2012.
- [29] I. Lee, E. Jeon, and J. Lee. On-site bioaerosol sampling and detection in microfluidic platforms. *TrAC Trends in Analytical Chemistry*, page 116880, 2022.
- [30] M. Li, L. Wang, W. Qi, Y. Liu, and J. Lin. Challenges and perspectives for biosensing of bioaerosol containing pathogenic microorganisms. *Micromachines*, 12(7):798, 2021.
- [31] Y. Li, X. Huang, I. Yu, T. Wong, and H. Qian. Role of air distribution in sars transmission during the largest nosocomial outbreak in hong kong. *Indoor air*, 15(2):83–95, 2005.
- [32] H. M. Mansour and A. J. Hickey. Raman characterization and chemical imaging of biocolloidal self-assemblies, drug delivery systems, and pulmonary inhalation aerosols: a review. *Aaps Pharmscitech*, 8:140–155, 2007.
- [33] L. Morawska, G. Buonanno, A. Mikszewski, and L. Stabile. The physics of respiratory particle generation, fate in the air, and inhalation. *Nature Reviews Physics*, 4:723–734, 11 2022.
- [34] G. Myhre, T. F. Berglen, M. Johnsrud, C. Hoyle, T. K. Berntsen, S. Christopher, D. Fahey, I. S. Isaksen, T. Jones, R. Kahn, et al. Modelled radiative forcing of the direct aerosol effect

- with multi-observation evaluation. *Atmospheric Chemistry and Physics*, 9(4):1365–1392, 2009.
- [35] G. Myhre, C. Myhre, B. Samset, and T. Storelvmo. Aerosols and their relation to global climate and climate sensitivity. *Nature Education Knowledge*, 4(5):7, 2013.
- [36] H. Priyamvada, K. Kumaragama, A. Chrzan, C. Athukorala, S. Sur, and S. Dhaniyala. Design and evaluation of a new electrostatic precipitation-based portable low-cost sampler for bioaerosol monitoring. *Aerosol Science and Technology*, 55(1):24–36, 2021.
- [37] R. G. Ramos, D. Libong, M. Rakotomanga, K. Gaudin, P. Loiseau, and P. Chaminade. Comparison between charged aerosol detection and light scattering detection for the analysis of leishmania membrane phospholipids. *Journal of Chromatography A*, 1209(1-2):88–94, 2008.
- [38] L. A. Remer, R. G. Kleidman, R. C. Levy, Y. J. Kaufman, D. Tanré, S. Mattoo, J. V. Martins, C. Ichoku, I. Koren, H. Yu, et al. Global aerosol climatology from the modis satellite sensors. *Journal of Geophysical Research: Atmospheres*, 113(D14), 2008.
- [39] M. Saros, R. Weber, J. Marti, and P. McMurry. Ultrafine aerosol measurement using a condensation nucleus counter with pulse height analysis. *Aerosol Science and Technology*, 25(2):200–213, 1996.
- [40] M. Sawano, K. Takeshita, H. Ohno, and H. Oka. Rt-pcr diagnosis of covid-19 from exhaled breath condensate: A clinical study. *Journal of Breath Research*, 15(3):037103, 2021.
- [41] G. Schweiger. Raman scattering on single aerosol particles and on flowing aerosols: a review. *Journal of aerosol science*, 21(4):483–509, 1990.
- [42] Y. Shen, J. M. Courtney, P. Anfinrud, and A. Bax. Hybrid measurement of respiratory aerosol reveals a dominant coarse fraction resulting from speech that remains airborne for minutes. *Proceedings of the National Academy of Sciences*, 119(26):e2203086119, 2022.
- [43] D. Sinclair and V. K. La Mer. Light scattering as a measure of particle size in aerosols. the production of monodisperse aerosols. *Chemical reviews*, 44(2):245–267, 1949.
- [44] T. Stakenborg, J. Raymenants, A. Taher, E. Marchal, B. Verbruggen, S. Roth, B. Jones, A. Yurt, W. Duthoo, K. Bombeke, et al. Molecular detection of sars-cov-2 in exhaled breath at the point-of-need. *Biosensors and Bioelectronics*, 217:114663, 2022.

- [45] R. Tellier. Covid-19: the case for aerosol transmission. *Interface Focus*, 12(2):20210072, 2022.
- [46] K.-A. Thompson, J. V. Pappachan, A. M. Bennett, H. Mittal, S. Macken, B. K. Dove, J. S. Nguyen-Van-Tam, V. R. Copley, S. O’Brien, P. Hoffman, et al. Influenza aerosols in uk hospitals during the h1n1 (2009) pandemic—the risk of aerosol generation during medical procedures. *PloS one*, 8(2):e56278, 2013.
- [47] N. Turgeon, M. Pagé, J. Robillard, V. Goulet, A. Bahloul, C. Brochot, M. N. Saidi, N. Dumont-Leblond, and C. Duchaine. Filtration performance, fit test and side effects of respiratory personal protective equipment following decontamination: Observations for user safety and comfort. *PLoS One*, 18(1):e0280426, 2023.
- [48] N. Turgeon, M.-J. Toulouse, B. Martel, S. Moineau, and C. Duchaine. Comparison of five bacteriophages as models for viral aerosol studies. *Applied and environmental microbiology*, 80(14):4242–4250, 2014.
- [49] A. E. Valsan, R. Ravikrishna, C. Biju, C. Pöhlker, V. Després, J. Huffman, U. Pöschl, and S. Gunthe. Fluorescent biological aerosol particle measurements at a tropical high-altitude site in southern india during the southwest monsoon season. *Atmospheric Chemistry and Physics*, 16(15):9805–9830, 2016.
- [50] N. Van Doremalen, T. Bushmaker, and V. Munster. Stability of middle east respiratory syndrome coronavirus (mers-cov) under different environmental conditions. *Eurosurveillance*, 18(38):20590, 2013.
- [51] D. Verreault, S. Moineau, and C. Duchaine. Methods for sampling of airborne viruses. *Microbiology and molecular biology reviews*, 72(3):413–444, 2008.
- [52] J. Wang, L. Yang, H. Wang, and L. Wang. Application of microfluidic chips in the detection of airborne microorganisms. *Micromachines*, 13(10):1576, 2022.
- [53] World Health Organization. Global health observatory data repository, 2021. Accessed on 2021-11-29.
- [54] M. Z. Zahir, J.-H. Lim, S.-Y. Noh, and S.-J. Yook. Development of electric virtual impactor with variable sampling particle size range. *Advanced Powder Technology*, 32(10):3456–3464, 2021.

- [55] Y. Zheng and M. Yao. Liquid impinger biosampler's performance for size-resolved viable bioaerosol particles. *Journal of Aerosol Science*, 106:34–42, 2017.